Full Title: **Cyfip2 controls the acoustic startle threshold through FMRP, actin polymerization, and $GABA_B$ receptor function.**

Short Title: **Cyfip2 controls startle sensitivity via FMRP, Rac1 and $GABA_B$ receptors.**

Jacob C. Deslauriers[1], Rohit P. Ghotkar[1,3], Lindsey A. Russ[1,4], Jordan A. Jarman[1,5], Rubia A. Martin[1,6], Rachel G. Tippett[1], Sureni H. Sumathipala[1], Derek F. Burton[1,7], D. Chris Cole[1], Kurt C. Marsden*[1,2]

1. Department of Biological Sciences, North Carolina State University, Raleigh, North Carolina, USA
2. Center for Human Health and the Environment (CHHE), North Carolina State University, Raleigh, North Carolina, USA
3. Current address: Putnam Associates, Boston, Massachusetts, USA
4. Current address: Department of Pharmacology & Physiology, Georgetown University, Washington D.C., USA
5. Current address: Department of Physiology and Biophysics, Boston University, Boston, MA, USA
6. Current address: U.S. Environmental Protection Agency, Raleigh-Durham-Chapel Hill, North Carolina, USA
7. Current address: Biogen, Durham, North Carolina, USA

*Corresponding author: kcmarsde@ncsu.edu

Author contributions: Conceptualization: JCD and KCM; Data curation: JCD, RAM; Formal analysis: JCD, RAM, RGT, SHS, DCC, KCM; Funding acquisition: KCM; Investigation: JCD, RPG, LAR, JAJ, RAM, RGT, SHS, DFB, DCC, KCM; Methodology: JCD, RAM, KCM; Project administration: KCM; Supervision: JCD, DFB, DCC, KCM; Visualization: JCD, RAM, KCM; Writing – original draft: JCD; Writing – review and editing: JCD, KCM

Abstract

Animals process a constant stream of sensory input, and to survive they must detect and respond to dangerous stimuli while ignoring innocuous or irrelevant ones. Behavioral responses are elicited when certain properties of a stimulus such as its intensity or size reach a critical value, and such behavioral thresholds can be a simple and effective mechanism to filter sensory information and determine if a response is appropriate. For example, the acoustic startle response is a conserved and stereotyped defensive behavior induced by sudden loud sounds, but dysregulation of the threshold to initiate this behavior can result in startle hypersensitivity that is associated with sensory processing disorders including schizophrenia and autism. Through a previous forward genetic screen for regulators of the startle threshold a nonsense mutation in *Cytoplasmic Fragile X Messenger Ribonucleoprotein (FMRP)-interacting protein 2* (*cyfip2*) was found that causes startle hypersensitivity in zebrafish larvae, but the molecular mechanisms by which Cyfip2 establishes the acoustic startle threshold are unknown. Here we use conditional transgenic rescue and CRISPR/Cas9 gene knockdown approaches to determine that Cyfip2 requires both Rac1 and FMRP pathways, but not the closely related FXR1 or FXR2, to regulate the acoustic startle threshold in early neurodevelopment. Using a candidate-based drug screen we find that Cyfip2 also acts acutely to maintain the startle threshold through Arp2/3-mediated branched actin polymerization and N-methyl D-aspartate receptors (NMDARs). To identify proteins and pathways that may be targets of Cyfip2-FMRP-mediated translational regulation, we then performed discovery proteomics and determined that loss of Cyfip2 alters cytoskeletal and extracellular matrix components and disrupts oxidative phosphorylation and GABA receptor signaling. Finally, we validated our proteomics findings by showing that the $GABA_B$ receptor agonist baclofen, but not the $GABA_A$ agonist muscimol, restores normal startle sensitivity in *cyfip2* mutants. Together, these data reveal that Cyfip2 acts through multiple pathways to regulate excitatory/inhibitory balance in the startle circuit to control the processing of acoustic information.

53 **Introduction**

54 To navigate their environments to find food and avoid predation, animals must be able to
55 filter out extraneous stimuli but respond appropriately to salient ones, a process known as
56 sensorimotor gating. Specific attributes of a stimulus can trigger a response; for visual stimuli
57 the luminance, size, and speed of the stimulus determine if escape and reorientation responses
58 are initiated [1–3]. Similarly, the intensity and frequency of acoustic stimuli determine whether a
59 response is made [4,5]. One way in which animals can control their responses to sensory stimuli
60 is by establishing a behavioral threshold such that when one or more of these stimulus
61 attributes reaches a critical value a specific behavioral response is initiated. Behavioral
62 thresholds are a fundamental mechanism of sensorimotor gating used across the animal
63 kingdom to regulate a wide range of behavioral responses including both collective responses,
64 such as fanning behaviors for hive climate regulation in bees [6,7] and shoaling behavior in fish
65 [8,9], as well as individual responses to odors [10–13], tactile stimuli [14–17], changes in
66 luminance and contrast of visual stimuli [1,18–21], and sound frequency and intensity in
67 mammals and fish [5,22–24]. That behavioral over-responsiveness to visual, tactile, and
68 acoustic stimuli is observed across a number of neuropsychiatric conditions including autism,
69 anxiety, and schizophrenia [4,22,24–28] highlights the importance of setting such behavioral
70 thresholds at an appropriate level. Yet our knowledge of the molecular mechanisms that both
71 establish and maintain behavioral thresholds is limited.

72 Previously, to identify genes that regulate the threshold for initiating the acoustic startle
73 response, a highly conserved behavior initiated following sudden loud sounds that may indicate
74 danger [5,29–31], we conducted a standard 3-generation, ENU-based forward genetic screen in
75 larval zebrafish [32]. We identified a set of five mutant lines that display acoustic startle
76 hypersensitivity, and through whole-genome sequencing of the *triggerhappy* mutant line, we
77 identified a causal, nonsense mutation in *cytoplasmic Fragile X Messenger Ribonucleoprotein*
78 *(FMRP)-Interacting protein 2* (*cyfip2).* Cyfip2 was first identified as an interactor of FMRP and

79 the elongation initiation factor 4E (eIF4E), through which it participates in translational
80 repression of many target transcripts [33,34]. Cyfip2, but not the closely related Cyfip1, can also
81 bind the Fragile X-related proteins FXR1 and FXR2, but the function of these interactions is
82 unknown [33]. Additionally, Cyfip2 interacts with the activated form of the small Rho GTPase
83 Rac1, and it is a member of the WAVE Regulatory Complex (WRC) in which it helps regulate
84 Arp2/3 activation and branched actin polymerization [35–41]. Cyfip2 is vital for proper neuronal
85 migration and cell movement, axonal growth and guidance, as well as synapse formation and
86 function in flies, mice, and zebrafish [32,33,37,42–47]. Homozygous *cyfip2* mutations are
87 embryonically lethal in mammals and fatal after 7-8 days post-fertilization (dpf) in zebrafish
88 [32,42,44,48]. Despite its key role in multiple aspects of neurodevelopment, the links between
89 how Cyfip2 regulates RNA translation, actin polymerization, and behavior have not been
90 defined. Our previous work demonstrated that loss of Cyfip2 causes acoustic startle
91 hypersensitivity that is reversible upon transgenic expression of GFP-tagged Cyfip2, alters the
92 morphology but not the electrophysiological properties of the startle command-like Mauthner
93 cells (M-cells), and causes hyperexcitability of the spiral fiber neurons (SFNs), a set of hindbrain
94 excitatory interneurons that project to the M-cell axon hillock [32]. It is unclear, however,
95 whether Cyfip2 acts via Rac1-mediated actin polymerization or through FMRP-mediated
96 translational repression to control the startle threshold. Furthermore, the downstream molecular
97 changes that directly modulate the function of the startle circuit have not been identified.
98 In this study we used an inducible rescue approach in *cyfip2* mutant zebrafish larvae to
99 demonstrate that both Cyfip2's Rac1 and FMRP interactions are required for establishing the
100 acoustic startle threshold during early neurodevelopment. Using CRISPR-Cas9 gene
101 knockdown we find that FXR1 and FXR2 are dispensable for startle regulation and that Cyfip2
102 acts through FMRP. Furthermore, with a candidate-based pharmacological approach we show
103 that Cyfip2 mediates Arp2/3-induced branched actin polymerization and may modulate N-
104 methyl-D-aspartate receptors (NMDARs) to alter neuronal function in the acoustic startle circuit.

105 Finally, we performed discovery proteomics to define molecular pathways disrupted by loss of
106 Cyfip2 *in vivo*. Our results indicate roles for Cyfip2 in mitochondrial function, oxidative
107 phosphorylation, and inhibitory Gamma-Aminobutyric Acid (GABA) receptor signaling. We
108 confirmed the functional importance of this last finding using the $GABA_B$ receptor agonist
109 baclofen, which rescues *cyfip2* mutants' hypersensitivity. Together these data establish a novel
110 pathway that links Cyfip2, actin dynamics, RNA translation, and excitatory/inhibitory balance in
111 the control of acoustic responsiveness.
112
113 **Results**
114 <u>Cyfip2 establishes the acoustic startle threshold through both Rac1 and FMRP.</u>
115 Cyfip2 has four known protein-interaction domains [49] (Fig. 1A), and it can act through
116 Rac1 to promote actin polymerization (Fig. 1B) and FMRP to regulate RNA translation (Fig. 1C).
117 *cyfip2*^{p400} mutants have a single base pair transversion (nt1024; T to A) resulting in a premature
118 stop codon at amino acid position 343 (Fig. 1A) [32]. *cyfip2*^{p400} mutant zebrafish larvae (5 dpf)
119 were previously shown to display acoustic startle hypersensitivity that could be rescued by
120 expressing Cyfip2 at 30 hours post fertilization (hpf) using a stable heatshock-inducible
121 transgenic line, *Tg(hsp70:cyfip2-EGFP)* [32]. We replicate those findings here, using a 60-
122 stimulus assay consisting of 10 trials at each of 6 intensities with a 20 second (s) interstimulus
123 interval (ISI) to measure startle sensitivity (Fig. 1D). A 40-min heatshock at 30 hpf restores
124 normal sensitivity in transgenic (*Tg*+) but not in non-transgenic (*Tg*-) *cyfip2* mutants (Fig. 1D,E).
125 Previous studies have established that C179R and K723E amino acid substitutions prevent
126 Cyfip2 from binding with Rac1 and FMRP, respectively [34,39,45]. To determine if Cyfip2
127 engages Rac1-mediated actin regulation and/or FMRP/eIF4E-mediated translational repression
128 pathways to establish the acoustic startle threshold, we induced C179R (Δ*Rac1*) and K723E
129 (Δ*FMRP*) point mutations in the *Tg(hsp70:cyfip2-EGFP)* construct and created stable transgenic
130 lines for each (Fig. 1A). We expressed either wildtype or mutant (Δ*Rac1*; Δ*FMRP)* versions of

131 Cyfip2 in mutants at 30 hpf with a 40-minute heatshock at 38°C, followed by acoustic startle
132 testing at 5 dpf. While expression of wildtype *Tg(hsp70:cyfip2-EGFP)* at 30 hpf rescues mutant
133 hypersensitivity, expression of Δ*Rac1* or Δ*FMRP* versions of Cyfip2 in mutants was insufficient
134 to rescue mutant hypersensitivity (Fig. 1E).

135 *cyfip2* mutants also display a number of kinematic defects in their performance of the
136 startle response [32]. To determine if Rac1 and FMRP binding are also required for Cyfip2 to
137 regulate startle kinematics, we analyzed startle latency, duration, head turn angle (C1 angle),
138 and total distance traveled during the response in *Tg*- and *Tg*+ fish after the same 40-min
139 heatshock protocol at 30 hpf (Fig. S1). Heatshock induction of wildtype Cyfip2 restored normal
140 latency, duration, and C1 angle, but not distance traveled (Fig. S1). All kinematic defects
141 remained in *cyfip2* mutant larvae expressing Δ*Rac1*-Cyfip2 (Fig. S1), but expression of Δ*FMRP*-
142 Cyfip2 was sufficient to rescue startle duration and induced a trend toward rescue of startle
143 latency and C1 turn angle (Fig. S1). These data suggest that Rac1 binding is required for all
144 aspects of Cyfip2-mediated startle regulation, while FMRP binding is required to regulate the
145 startle threshold but is largely dispensable for startle kinematics.

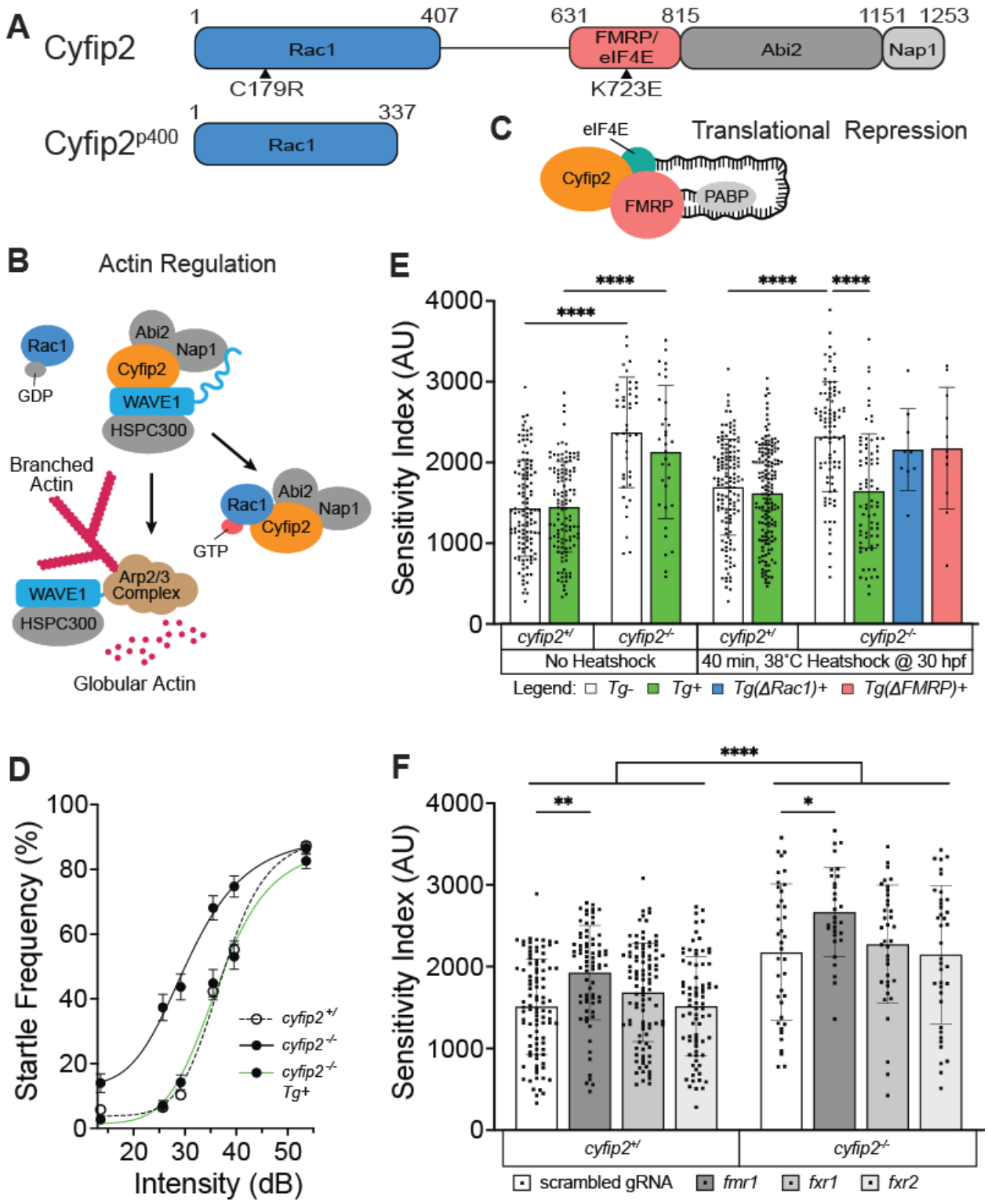

Figure 1. Cyfip2 establishes the acoustic startle threshold through Rac1 and FMRP. (A) Cyfip2 protein interacting domain diagram of wildtype (top) and mutant (bottom) Cyfip2 proteins. Black arrowheads indicate the positions of induced mutations in Cyfip2, eliminating the Rac1- (C179R) or FMRP/eIF4E (K723E)-binding capacity of Cyfip2. (B) Cyfip2 actin regulatory pathway wherein Cyfip2 (orange) upon stimulation by Rac1-GTP triggers WAVE1 activation, Arp2/3-complex initiation and branched actin nucleation. (C) Cyfip2 translational repression pathway in which Cyfip2, eIF4E (teal), and

153 FMRP (pink) along with the poly-A binding protein (PABP; gray), sequester neurodevelopmentally
154 important mRNAs from being translated. (D) Average startle frequency (%) after 10 trials at 13.6, 25.7,
155 29.2, 35.5, 39.6 and 53.6 dB for 5 dpf *cyfip2* siblings (+/) and mutant (-/-) larvae heatshocked at 30 hpf for
156 40 minutes at 38˚C. The average startle frequency curve for *cyfip2* siblings (+/; open circles, dashed line),
157 *cyfip2* mutants (-/-; closed circles, solid line) and *cyfip2* mutants harboring the *Tg(hsp70:cyfip2-EGFP)+*
158 transgene (-/-; Tg+; closed circles, solid green line). (E) Sensitivity indices, calculated as the area under
159 the startle frequency curves, for 5 dpf *cyfip2* siblings and mutants, following a 40-minute heatshock at 30
160 hpf to express either wildtype (*Tg+*; green), Rac1- (Δ*Rac1+*; blue) or FMRP/eIF4E- (Δ*FMRP+*; pink)
161 binding deficient versions of Cyfip2-EGFP. Comparisons were made to both non-transgenic (*Tg-*) and
162 non-heatshocked controls. All indices (mean ± SD) compared using a Kruskal-Wallis test with Dunn's
163 multiple comparisons correction; p**** < 0.0001. (F) Sensitivity indices for 5 dpf *cyfip2* sibling (+/) and
164 mutant (-/-) larvae following 1-cell stage injection with CRISPR-Cas9 and a single, *scrambled* guide RNA
165 (gRNA) or dual gRNA cocktails targeting *fmr1*, *fxr1,* or *fxr2*. *scrambled* gRNA injected (white bar, closed
166 circles); *fmr1* gRNA injected (dark gray bar closed circles); *fxr1* gRNA injected (medium gray bar; closed
167 circles); *fxr2* gRNA injected (light gray bar, closed circles). Comparisons were made both within genotype
168 and between genotypes by condition. All indices (mean ± SD) compared using an Ordinary one-way
169 ANOVA with Sidak's multiple comparisons correction; p* < 0.05; p** < 0.01; p**** < 0.0001.
170

171 One possible explanation for these results is that expression levels may differ between
172 the three heatshock transgenic lines. We therefore measured expression levels of each
173 transgenic Cyfip2-GFP protein 6 hours after a 40-min heatshock by fluorescence intensity (Fig.
174 S2A). The Δ*Rac1* and Δ*FMRP* lines displayed GFP expression that was not significantly
175 different than the wildtype *Tg+* line but which trended lower. To induce expression of wildtype
176 Cyfip2-GFP at levels more comparable to the Δ*Rac1* and Δ*FMRP* lines after 40-minute
177 heatshock, we delivered a 15-min heatshock at 30 hpf in the wildtype *Tg+* line. The 15-min
178 heatshock reduced peak Cyfip2-GFP expression to levels comparable to or below that of the
179 Δ*Rac1* and Δ*FMRP* lines, and this level of expression was also sufficient to rescue acoustic
180 startle sensitivity in *cyfip2* mutants (Fig. S2A-C). Thus, the level of transgene expression cannot
181 account for the failure of the Δ*Rac1* and Δ*FMRP* constructs to rescue startle phenotypes, and
182 these findings support our conclusion that Cyfip2 utilizes both Rac1- and FMRP-mediated
183 pathways to establish the acoustic startle threshold.
184

185 <u>Cyfip2 acts through FMRP but not FXR1/2 to establish the acoustic startle threshold.</u>

186 We previously found that FMRP is not required to establish a normal startle threshold, as
187 *fmr1*^{hu2787} mutants' startle sensitivity is unaffected [32]. Having established that the K723 residue

188 that Cyfip2 uses to bind FMRP is required for normal startle sensitivity, however, we
189 hypothesized that Cyfip2 may instead interact with other members of the Fragile X protein
190 family, Fragile X-related proteins 1 and 2 (FXR1/2), to establish the acoustic startle threshold
191 [33]. We designed pairs of CRISPR guide RNAs (gRNAs) targeting each of the *fmr1, fxr1* and
192 *fxr2* genes. We injected *fmr1*-, *fxr1*- or *fxr2*-specific CRISPR-Cas9 cocktails into 1-cell stage
193 *cyfip2* sibling and mutant embryos and measured acoustic startle sensitivity in these crispant
194 larvae at 5 dpf (Fig. 1F). Highly efficient CRISPR-induced mutagenesis was observed for all 3
195 genes, with 4 of the 6 gRNAs inducing edits as confirmed by PCR amplification and Sanger
196 sequencing (Fig. S3A-F). Quantitative PCR confirmed that mRNA expression of all three genes
197 was strongly reduced by CRISPR/Cas9 injection (Fig. S3G). FMRP crispants had significantly
198 increased startle sensitivity compared to larvae injected with a scrambled gRNA plus Cas9, and
199 sensitivity of FMRP crispants was even further increased in the *cyfip2* mutant background (Fig.
200 1F). However, startle sensitivity was unaltered in FXR1 or FXR2 crispants in either *cyfip2*
201 siblings or mutants (Fig. 1F). These data indicate that FMRP, but not FXR1/2, regulates the
202 startle threshold. The discrepancy between our hypersensitive FMRP crispants and prior
203 analysis of non-hypersensitive mutants from the ENU-induced *fmr1*^{hu2787} line is likely due to the
204 different methods used to generate these lines. Indeed, a recent study has shown that there is
205 substantial genomic adaptation in the *fmr1*^{hu2787} mutant line that may partially compensate for
206 the loss of FMRP [50], and an independently created CRISPR-induced *fmr1* mutant line
207 displayed additional behavioral and developmental phenotypes not seen in the *fmr1*^{hu2787} line
208 [51]. Thus, together with these findings our data indicate that Cyfip2 acts in part through FMRP
209 to establish the startle threshold.
210
211 <u>Cyfip2 maintains the acoustic startle threshold through Rac1 and FMRP pathways throughout</u>
212 <u>early neurodevelopment.</u>

Our previous study found that Cyfip2 is important for both establishing the acoustic startle threshold during early neurodevelopment, and for actively modulating the threshold later in development between 4 and 6 dpf [32]. Here we sought to define a critical window for Cyfip2 expression in regulating the startle threshold using our heatshock transgenic lines. Our results show that while a 40-minute heatshock to induce expression of wildtype Cyfip2 (*Tg*+) at 30 hpf is sufficient for behavioral rescue in 5 dpf *cyfip2* mutant larvae (Fig. 1D,E), a 40-min heatshock at 2, 3, or 4 dpf fails to rescue *cyfip2* mutant hypersensitivity (Fig. S4). Heatshock-induced expression at 5 dpf, 4 hours prior to testing, resulted in a trend toward rescue and a bi-modal distribution with some *cyfip2* mutants remaining hypersensitive and a second population showing restoration of normal sensitivity (Fig. 2A). These results are similar to our prior findings [32], and they suggest that Cyfip2 can not only function in the development of the startle circuit but can also actively maintain the circuit's threshold after it has formed. Next, to determine if Cyfip2 employs both of its canonical pathways in maintaining the startle threshold after 4 dpf, we expressed either Δ*Rac1* or Δ*FMRP* versions of Cyfip2 in *cyfip2* mutants at 5 dpf with a 40-min heatshock followed by acoustic startle behavior testing 6 hours later. Similar to what we observed with the developmental heatshock (Fig. 1E), neither expression of Δ*Rac1* nor ΔFMRP Cyfip2 at 5 dpf rescued acoustic hypersensitivity in mutants (Fig 2A). These findings suggest that Cyfip2 uses both its Rac1- and FMRP-mediated pathways to both establish and dynamically maintain the acoustic startle threshold throughout neurodevelopment.

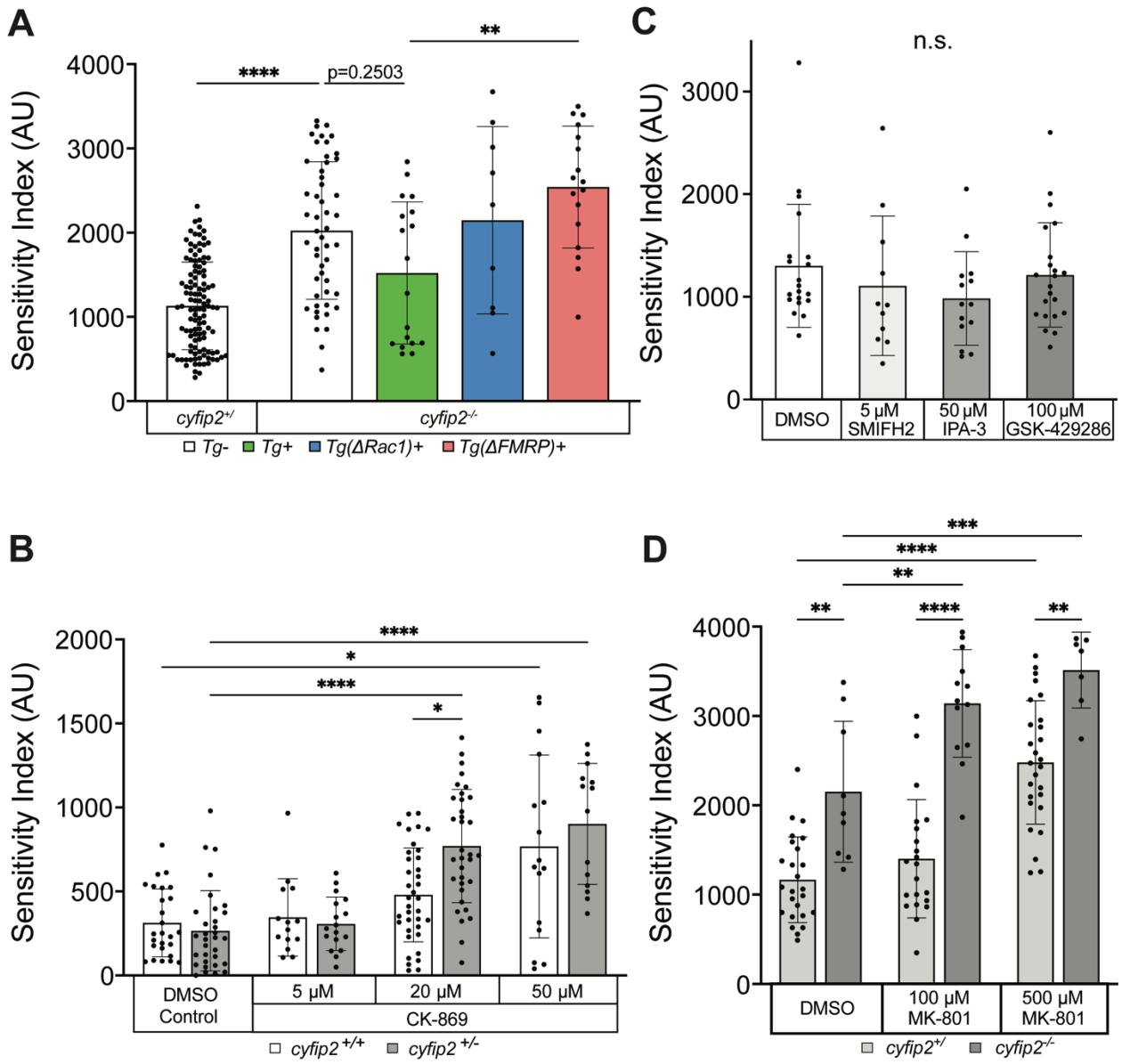

Figure 2. Cyfip2 acutely regulates branched actin polymerization and NMDARs to establish the acoustic startle threshold. (A) Sensitivity indices for 5 dpf *cyfip2* sibling (+/) and mutant (-/-) larvae, following a 40-minute heatshock at 120 hpf (5 dpf) to express either wildtype (*Tg*+; green), Rac1- (Δ*Rac1*+; blue) or FMRP/eIF4E- (Δ*FMRP*+; pink) binding deficient versions of Cyfip2-EGFP. Comparisons were made to non-transgenic (*Tg*-), heatshocked sibling (+/) and mutant (-/-) controls. All indices (mean ± SD) compared using a Kruskal-Wallis test with Dunn's multiple comparisons correction; p-values listed; p** < 0.01, p**** < 0.0001. (B) Sensitivity indices for 5 dpf *cyfip2* wildtype (+/+; white bar) and heterozygous (+/-; gray bar) larvae, treated for 30 minutes on d5 with 5, 20 or 50 μM CK-869. Comparisons were made both within genotype and within condition. All indices (mean ± SD) compared using a Kruskal-Wallis test with Dunn's multiple comparisons correction; p* < 0.05; p**** < 0.0001. (C) Sensitivity indices for 5 dpf Tüpfel longfin (TLF) larvae treated for 30 minutes on d5 with the highest, non-lethal doses the formin antagonist (SMIFH2; 5 μM), PAK3 antagonist (IPA-3; 50 μM) and ROCK antagonist (GSK429286; 100 μM). Comparisons were made between respective treatments and the DMSO controls. All indices (mean ± SD) were compared using a Kruskal-Wallis test with Dunn's multiple comparisons correction; All comparisons made were non-significant (n.s.). (D) Sensitivity indices for 5 dpf *cyfip2* sibling (+/) and mutant (-/-) larvae, treated for 30 minutes on d5 with 100 or 500 μM MK-801.

Comparisons were made both between genotypes within condition and between conditions by genotype. All indices (mean ± SD) were compared using an Ordinary one-way ANOVA with Tukey's multiple comparisons correction. $p^{**} < 0.01$; $p^{***} < 0.001$; $p^{****} < 0.0001$.

Cyfip2 maintains the acoustic startle threshold through branched actin polymerization.

Regulation of the actin cytoskeleton is a vital cellular process that within the context of the nervous system is critical for cell migration and movement, synapse formation, function and plasticity, receptor anchoring and trafficking, as well as axon growth and guidance [52]. Given our findings that Cyfip2 can act through the Rac1-WAVE pathway to establish and modulate the acoustic startle threshold, we hypothesized that Cyfip2-mediated branched actin polymerization specifically modulates the startle threshold. To test this hypothesis, we incubated 5 dpf *cyfip2* heterozygous and wildtype larvae in the Arp2/3 antagonist CK-869 at 5, 20, or 50 μM for 30 minutes, followed by acoustic startle testing. In control conditions, *cyfip2* heterozygotes display startle sensitivity equal to that of wildtypes (Fig. 2B), and incubation at 5 μM did not significantly alter startle sensitivity of either heterozygotes or wildtypes (Fig 2B). At 20 μM, wildtype larvae are unaffected by CK-869, but *cyfip2* heterozygotes have significantly increased startle sensitivity compared to controls (Fig 2B). 50 μM CK-869 caused both *cyfip2* wildtype and heterozygous larvae to become significantly hypersensitive compared to controls, phenocopying *cyfip2* mutants. Thus, Arp2/3-mediated, branched actin polymerization is necessary for acutely maintaining the acoustic startle threshold. That *cyfip2* heterozygotes display hypersensitivity at 20 μM but wildtypes do not indicates that a single functional copy of *cyfip2* is insufficient to maintain normal startle circuit function when branched actin polymerization is limited by a moderate dose of CK-869. We found similar results when exposing larvae to another Arp2/3 antagonist, CK-666, with both *cyfip2* heterozygotes and wildtypes phenocopying mutant hypersensitivity at a 50 μM concentration (Table S2). These findings support the conclusion that Cyfip2-dependent Arp2/3-mediated branched actin polymerization is necessary to maintain the acoustic startle threshold.

277 The actin cytoskeleton is dynamic and requires the action of both branched and
278 unbranched actin regulatory pathways to maintain cellular structure and function. Unbranched
279 filamentous (F) actin is polymerized from globular actin monomers by dimeric complexes of
280 formin proteins, which bind at the barbed ends of new filaments and promote their elongation
281 [53–56]. Another form of actin regulation involves the action of cofilin, an actin severing protein
282 that cleaves existing filaments to create new barbed ends and increase the rate of actin turnover
283 within the cell [57]. To determine whether unbranched actin and severing pathways play a role
284 in regulating the acoustic startle threshold we incubated 5 dpf wildtype larvae in a formin
285 antagonist, SMIFH2, or the cofilin disinhibitors, IPA-3 and GSK429286, for 30 minutes followed
286 by acoustic startle testing. Treatment with 5 μM SMIFH2 or with 50 μM IPA-3 or 100 μM
287 GSK429286 did not significantly affect startle sensitivity in wildtype larvae (Fig 2C). We also
288 tested these drugs at higher concentrations, which were lethal after a 30-minute exposure, as
289 well as longer exposures at lower concentrations, which had no effect on startle sensitivity
290 (Table S1). Our data with the formin inhibitor SMIFH2 are in contrast to a recent finding showing
291 that Formin 2B morpholino knockdown caused a decrease in Mauthner cell-mediated fast startle
292 responses in zebrafish larvae [58]. That we did not observe any change in startle frequency is
293 likely due to the acute nature of our pharmacological approach as opposed to the morpholino-
294 mediated developmental knockdown of Formin 2B. Our findings suggest that acute
295 perturbations to unbranched actin filaments and actin turnover do not play a significant role in
296 regulating the acoustic startle threshold. Altogether these data further support our conclusion
297 that Cyfip2-mediated, branched actin polymerization is a key pathway for acutely maintaining
298 the acoustic startle threshold.
299
300 <u>Cyfip2 may regulate NMDA receptors to modulate the acoustic startle threshold.</u>
301 While we have established that Cyfip2 mediates the establishment and maintenance of
302 the acoustic startle threshold through both branched actin and FMRP regulatory pathways, it is

303 unclear what molecular mechanisms directly modulate the excitability of the startle circuit. To
304 identify molecules that may be downstream effectors of Cyfip2 in modulating activity of the
305 startle circuit, we conducted a candidate-based small-molecule screen with compounds
306 previously shown to alter startle sensitivity in wildtype zebrafish larvae (Table 1) [59]. In this
307 screen we incubated *cyfip2* wildtype, heterozygous, and mutant larvae in each compound for 30
308 min prior to and during acoustic startle testing. Consistent with previous findings, *N*-
309 phenylanthrinilic acid (NPAA; Cl^- channel antagonist), Meclofenamic acid (MA; K^+ channel and
310 gap junction antagonist), Phenoxybenzamine (POBA; alpha-adrenergic receptor and calmodulin
311 antagonist), Etazolate (ETAZ; phosphodiesterase 4 (PDE4) inhibitor), and MK-801 (N-methyl-D-
312 aspartate receptor (NMDAR) antagonist) all increased startle sensitivity in a dose-dependent
313 manner (Table 1). BMS204352, a different K^+ channel antagonist, did not alter acoustic startle
314 sensitivity at either 10 or 50 μM concentrations, and NSC-23766, a Rac1 antagonist, reduced
315 sensitivity in siblings at 100 μM, but not *cyfip2* mutants.
316

Compound	Concentration (μM)	Effect By Genotype		
		cyfip2(+/+)	***cyfip2(+/-)***	***cyfip2(-/-)***
NPAA (Cl-channel antagonist)	1	93.21% of Control, p > 0.99	110.21% of Control, p < 0.99	113.57% of Control, p > 0.99
	5	140.11% of Control, p = 0.9785	137.32% of Control, p = 0.1385	140.29% of Control, p > 0.2787
	10	**234.14% of Control, p** = 0.0038**	**201.29% of Control, p**** < 0.0001**	**155.06% of Control, p* = 0.0189**
MA (K+ channel/gap jxn. antagonist)	1	131.6% of Control, p > 0.99	11.87% of Control, p > 0.99	132.29% of Control, p = 0.5732
	5	137.24% of Control, p > 0.99	138.46% of Control, p = 0.0622	112.29% of Control, p > 0.99
	10	214.13% of Control, p = 0.0833	**169.81% of Control, p* = 0.0188**	**155.76% of Control, p* = 0.0288**
POBA (AAR/calmodulin antagonist)	1	102.9% of Control, p > 0.99	107.08% of Control, p > 0.99	101.04% of Control, p > 0.99
	10	136.17% of Control, p > 0.99	106.58% of Control, p > 0.99	99.01% of Control, p > 0.99
	50	**175.8% of Control, p* = 0.0123**		99.76% of Control, p > 0.99
ETAZ (PDE4 inhibitor)	1	141.79% of Control, p > 0.99	126.36% of Control, p > 0.99	121.74% of Control, p > 0.99
	10	168.6% of Control, p = 0.5472	**172.26% of Control, p* = 0.0137**	152.73% of Control, p = 0.3977

	50	**236.64% of Control, p** = 0.0029**	**179.99% of Control, p** = 0.0015**	**149.75% of Control, p* = 0.0105**
MK-801 (NMDAR antagonist)	100	120.19% of Control, p > 0.99		**145.93% of Control, p** = 0.0024**
	500	**212.69% of Control, p**** < 0.0001**		**163.26% of Control, p*** = 0.0002**
BMS-204352 (K+ channel antagonist)	10	79.48% of Control, p = 0.4269		89.55% of Control, p > 0.99
	50	76.08% of Control, p = 0.6759		108.74% of Control, p > 0.99
NSC-23766 (Rac1 antagonist)	100	**49.14% of Control, p*** = 0.0002**		81.60% of Control, p > 0.99
	200	86.26% of Control, p > 0.99		105.28% of Control, p > 0.99

Table 1. Cyfip2 may regulate NMDARs to control acoustic startle sensitivity. Mean startle index comparisons, listed as percentage (%) of the mean startle index of vehicle-treated controls by *cyfip2* genotype and drug concentration, for larvae treated with compounds targeting the indicated pathways [59] to increase acoustic startle sensitivity. All significant differences ($p < 0.05$) are listed (**bold**) for comparisons using a Kruskal-Wallis test and Dunn's multiple comparisons correction. NPAA (*N*-phenylanthranilic acid); MA (meclofenamic acid); POBA (phenoxybenzamine); ETAZ (etazolate).

To determine whether any of the targeted pathways may be downstream of Cyfip2, we looked for conditions in which there was a clear *cyfip2* genotype-specific effect on sensitivity. The NMDA receptor blocker MK-801 showed the clearest such effect, with a low dose (100 μM) elevating startle sensitivity only in *cyfip2* mutants but not siblings (Table 1). Therefore, Cyfip2-mediated cytoskeletal and/or translational regulation may impact the expression and/or function of NMDA receptors within the startle circuit to modulate the acoustic startle threshold.

<u>Proteomic analysis reveals that Cyfip2-mediated regulation of $GABA_B$ receptors is critical for startle sensitivity.</u>

To complement our candidate drug screen with an unbiased approach to identify proteins and molecular pathways regulated by Cyfip2, likely through its role in translational regulation, we conducted a proteomic analysis of *cyfip2* wildtype, heterozygous, and mutant larvae at 5 dpf. All larvae used were siblings and were genotyped by PCR and Sanger sequencing and then pooled in groups of 30 per genotype and snap frozen with liquid nitrogen. Three independent pools of 30 larvae were analyzed for each genotype. Protein lysates were submitted to the Molecular Education, Technology and Research Innovation Center (METRIC)

340 at NC State University for protein digestion and LC-MS. Raw LC-MS files were processed and
341 quantified using MaxQuant (Max Planck Institute of Biochemistry) and imported into Perseus
342 software for transformation and identification of Differentially Expressed Proteins (DEPs) for
343 subsequent Ingenuity Pathway Analysis (IPA).

344 Comparative analysis of *cyfip2* heterozygous and mutant versus wildtype proteomes
345 identified a total of 221 differentially expressed proteins (DEPs) in heterozygotes and 127 DEPs
346 in mutants (Fig. S5A-B; Tables S7,S8). Cyfip2 was the most strongly downregulated protein in
347 mutants, providing a key validation of our approach (Fig. 3A,S5A; Tables S7,S8). Cyfip2 was
348 slightly but significantly downregulated in heterozygotes as well (Fig. S5B), providing a basis for
349 the sensitization of Cyfip2 heterozygotes to the actin inhibitor CK-869 (Fig. 2B). Cyfip1
350 expression was not significantly altered in either genotype, indicating that it likely does not act to
351 compensate for the loss of Cyfip2 (Fig. S5A-B). 66 DEPs were shared between *cyfip2*
352 heterozygotes and mutants, while 155 and 61 DEPs were specific to each group, respectively
353 (Fig. S5C). The top 5 upregulated proteins identified in *cyfip2*^{p400} heterozygotes in descending
354 order included: microtubule actin cross-linking factor 1 (MACF1), acyl-CoA dehydrogenase
355 family member 11 (ACAD11), cullin 2 (CUL2), calcium channel, voltage dependent, L-type alpha
356 1S (CACNA1S) and ubiquitin specific peptidase 24 (USP24) (Fig. 3A; top, green). The top 5
357 downregulated proteins identified in *cyfip2*^{p400} heterozygotes in descending order included:
358 tyrosine 3-monooxygenase/tryptophan 5-monooxygenase activation protein theta or 14-3-3
359 protein theta (YWHAQ), SEC61 translocon subunit alpha 1 (SEC61A1), ribosomal protein S5
360 (RPS5), enolase 2 (ENO2), and ribosomal protein L18A (RPL18A) (Fig 3A; top, red). The top 5
361 upregulated proteins identified in *cyfip2*^{p400} mutants in descending order included: ACAD11,
362 mitochondrial NADH dehydrogenase 4 (MT-ND4), NIPBL cohesion loading factor b (NIPBL),
363 troponin C2 fast skeletal type (TNNC2), and USP24 (Fig 3A; bottom, green). The top 5
364 downregulated proteins identified in *cyfip2*^{p400} mutants in descending order included:
365 cytoplasmic FMR1-interacting protein 2 (CYFIP2), collagen type VI alpha 3 (COL6A3), stress-

366 induced phosphoprotein 1 (STIP1), thymosin beta (TMSB10/TMSB4X) and collagen type 1
367 alpha 1 (COL1A1) (Fig 3A; bottom, green). These changes highlight the diverse set of roles that
368 Cyfip2 plays, impacting translational machinery, metabolism, and the extracellular matrix.
369 IPA analysis of DEPs in *cyfip2* heterozygotes and mutants revealed disruption of
370 multiple pathways common to both genotypes. Notable disrupted pathways shared between
371 *cyfip2* heterozygotes and mutants include oxidative phosphorylation, mitochondrial dysfunction,
372 EIF2 signaling, sirtuin signaling, eIF4/p70S6K signaling, 14-3-3-mediated signaling, and GABA
373 receptor signaling (Fig. 3B). Analysis of the most affected diseases and functions for each
374 genotype supports a role for Cyfip2-mediated regulation in neuromuscular disease, disorder of
375 the basal ganglia, dyskinesia, Huntington disease, breast cancer, familial encephalopathy, and
376 neurological disorders (Fig. 3C). These data provide further evidence of the central importance
377 of Cyfip2 for neural function.
378 Finally, we sought to confirm that these pathways play a functional role in regulating
379 startle sensitivity, and so we focused on GABA receptor signaling as the likeliest to contribute to
380 the hyperexcitability of *cyfip2* mutant larvae. We applied agonists of both ionotropic $GABA_A$
381 receptors (muscimol) and metabotropic $GABA_B$ receptors (baclofen) for 1 hour prior to startle
382 testing. Muscimol did not have a consistent impact on mutant hypersensitivity at 1, 10, or 100
383 μM (Fig. 3D), but baclofen induced a clear restoration of normal sensitivity in *cyfip2* mutants at
384 10 μM (Fig. 3E). Importantly, baclofen application did not affect startle sensitivity in sibling
385 larvae. Thus, Cyfip2 maintains a normal startle threshold by promoting GABAergic inhibition
386 through the activity of $GABA_B$ receptors. Together our findings establish a set of molecular
387 pathways downstream of Cyfip2 that enable the proper processing of acoustic stimuli to limit
388 sensory over-responsiveness.
389

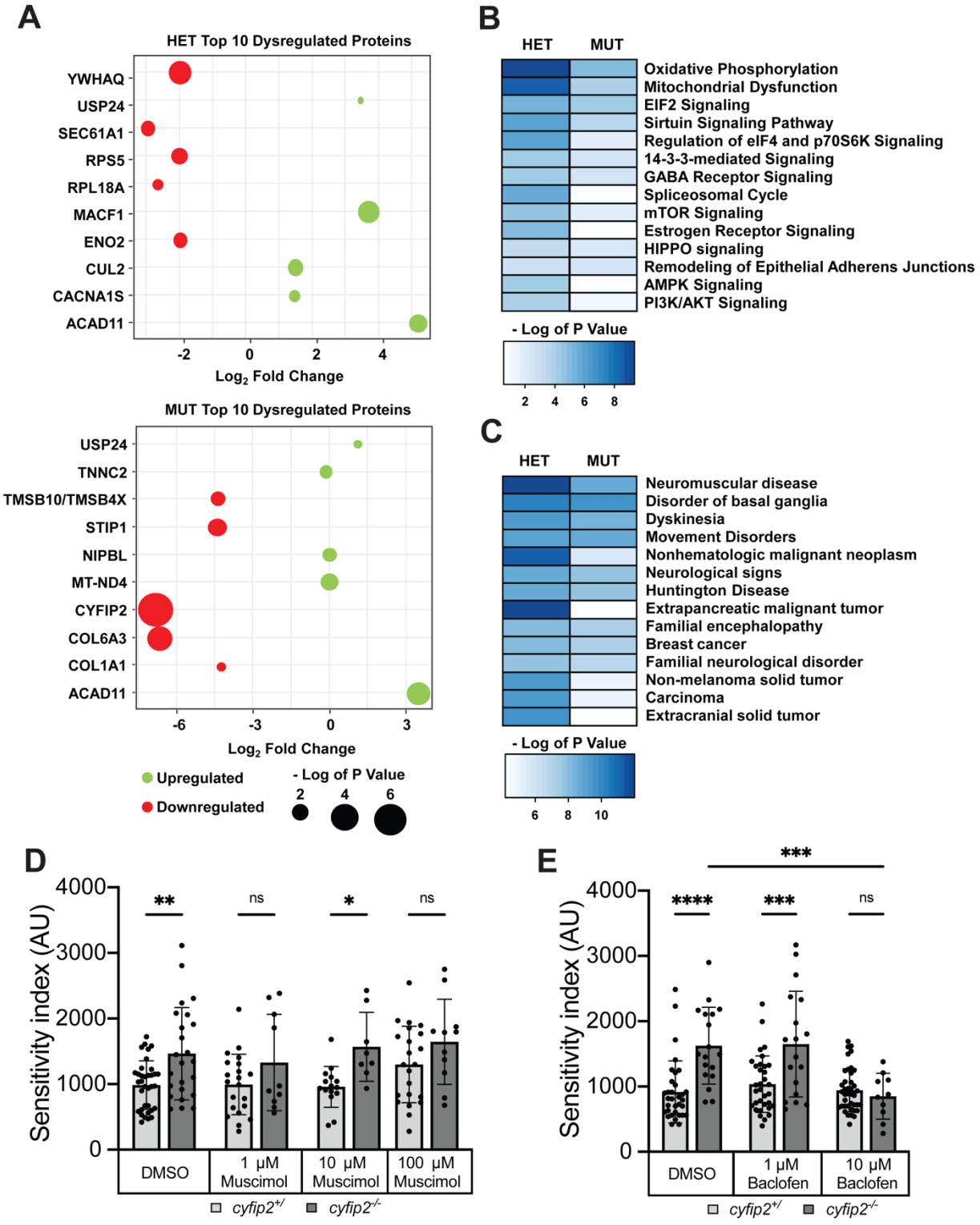

Figure 3. Loss of Cyfip2 causes widespread proteomic changes and $GABA_B$ receptor signaling is critical for startle sensitivity. (A) Bubble plots reporting the level of significance of the top 10 dysregulated proteins for both *cyfip2* heterozygous (top) and mutant (bottom) groups compared to wildtype controls. The size of the dot is proportional to the significance of the results while the color code represents the $\log_2$ fold change; top five upregulated (green), and top five downregulated (red) proteins

396 are shown. (B-C) Heat maps displaying the impacted canonical pathways (B) and diseases and biological
397 functions (C) from IPA functional analysis. The blue-colored gradient indicates the degree of enrichment
398 for the listed pathways or diseases/functions, as represented by the – log of the P value for each
399 pathway, disease and/or function. (D-E) Sensitivity indices for 5 dpf *cyfip2* sibling (+/) and mutant (-/-)
400 larvae, treated for 60 minutes prior to testing with muscimol (D) or (E) baclofen. All indices (mean ± SD)
401 were compared using a one-way ANOVA with Sidak's multiple comparisons correction. $p^* < 0.05$, $p^{**} <$
402 0.01; $p^{***} < 0.001$; $p^{****} < 0.0001$.

403

404 **Discussion**

405 Through its ability to modulate both the actin cytoskeleton and protein translation, Cyfip2
406 is well-positioned to be a critical factor for many processes in neurodevelopment [33,34,37–
407 39,45,49]. Further highlighting its importance, Cyfip2 has been implicated in an array of
408 neuropsychiatric and other conditions, including schizophrenia [60], autism [49,61–63], binge
409 eating [64–66], obesity [67], amyotrophic lateral sclerosis (ALS) [68,69], Alzheimer's disease
410 [70], epilepsy [63,71–74], and cancer [75–80]. Here we focused on Cyfip2's role in a common
411 endophenotype of schizophrenia and autism, increased acoustic startle responsiveness
412 [4,24,27,28]. By combining conditional transgenesis, CRISPR/Cas9 gene editing,
413 pharmacology, and discovery proteomics in an *in vivo*, vertebrate model system, we found that
414 both actin and translational regulation pathways are required for Cyfip2 to establish and
415 maintain a normal startle threshold. Our data indicate that through these pathways Cyfip2
416 regulates both excitatory (NMDA receptor) and inhibitory ($GABA_B$ receptor) function to establish
417 and maintain proper sensory responsiveness.

418

419 Cyfip2 acts through both Rac1 and FMRP to establish the acoustic startle threshold.

420 The actin regulating function of Cyfip2-Rac1 interactions is essential for many
421 neurodevelopmental processes including neuronal outgrowth and maturation, synapse
422 formation and function, axon guidance and cell migration [38,44,45,81]. The functional
423 importance of Cyfip2-FMRP interactions, though less well characterized than Cyfip1-FMRP
424 interactions, are thought to similarly impact the expression of many key neurodevelopmental

425 proteins that are directly involved in axon growth, synapse maturation, and synaptic plasticity
426 [34,45,82–84]. Here we used a heatshock-inducible expression system to reveal that Cyfip2
427 requires the ability to interact with both Rac1 and FMRP to establish the acoustic startle
428 threshold early in neurodevelopment (Fig. 1E). The ability of wildtype Cyfip2 to restore normal
429 startle sensitivity in mutant larvae when expression is induced at 30 hpf (Fig. 1D,E), but not at
430 48, 72, or 96 hpf (Fig. S4) reveals some potential ways that it may affect the underlying neural
431 circuits. Prior to the rescue window, by 8-15 hpf the command-like Mauthner cells have been
432 specified [85] and begun extending their axons (17-18 hpf) and lateral dendrites (22-23 hpf)
433 [86,87]. During the rescue window from ~30-48 hpf, other neurons in the startle circuit continue
434 to migrate to their final positions in the ventral hindbrain, and the synaptic contacts within the
435 circuit begin to form and mature, including those between the auditory nerve, Mauthner cells,
436 and excitatory Spiral Fiber Neurons (SFNs) [87–89]. Actin dynamics would be required during
437 this time to facilitate neuronal migration, axon and dendrite growth, and synapse formation.
438 These processes would also require precisely regulated RNA translation through complexes like
439 Cyfip2-FMRP-eIF4E to produce the many proteins needed to establish these connections.
440 When we induced Cyfip2 expression at 5 dpf we observed a clear bimodal distribution with
441 some mutants remaining hypersensitive and a second population with normal sensitivity (Fig.
442 2A). This pattern was not observed when Rac1 or FMRP binding was abolished, suggesting that
443 both pathways are also needed for Cyfip2 to modulate the startle circuit in this acute context,
444 which would likely occur through changes in neuronal and/or synaptic function rather than
445 altered connectivity. That Cyfip2 expression between 48-96 hpf did not restore the startle
446 threshold in mutants could be due to insufficient expression levels, but together our conditional
447 expression experiments more likely indicate that Cyfip2 is able to most reliably function when
448 the circuit is in a less mature state.
449 Our findings also show that Cyfip2-Rac1 but not Cyfip2-FMRP binding is required for the
450 performance of the startle response, as kinematic parameters including latency, turn angle, and

451 duration were largely restored to normal by wildtype and Δ*FMRP* versions of Cyfip2 but
452 remained altered in Δ*Rac1*-Cyfip2 expressing *cyfip2* mutants (Fig. S1). These data demonstrate
453 that the actin regulation and translation regulation functions of Cyfip2, while both are required in
454 some contexts, also have some non-overlapping roles. This is consistent with findings in
455 zebrafish larvae showing that Cyfip2's interaction with FMRP is dispensable but that its
456 interaction with the Wave Regulatory Complex (WRC), which like the Rac1-Cyfip2 interaction
457 regulates actin polymerization (Fig. 1B), is required for retinal ganglion cell (RGC) axons to
458 properly navigate to their targets in the contralateral optic tectum [45]. In the startle context, our
459 data showing that Δ*FMRP*-Cyfip2 drives a stronger rescue for turn angle and duration than for
460 latency suggest that the Cyfip2-FMRP translational regulation pathway contributes more to the
461 initial sensory processing of acoustic stimuli than the regulation of motor output in the spinal
462 cord. The actin regulatory function of Cyfip2, however, appears to be critical for all of Cyfip2's
463 known roles in the startle circuit.
464
465 <u>Cyfip2-dependent startle threshold regulation requires FMRP but not FXR1/2.</u>
466 Previously, we observed that mutants from the *fmr1*^{hu2787} line have normal startle
467 sensitivity, suggesting that FMRP plays no role in regulating the startle threshold [32]. So here
468 we tested whether Cyfip2, which in contrast to the closely related Cyfip1 has the capacity to also
469 bind with the Fragile X-related proteins FXR1 and FXR2 [33], may instead rely on these binding
470 partners to modulate the startle threshold. Like FMRP, both FXR1 and FXR2 regulate RNA
471 translation [90,91] and are expressed in the brain during early vertebrate neurodevelopment,
472 though divergent expression patterns emerge for the FXR1/2 proteins in later development and
473 adulthood in most vertebrates [92–94]. By analyzing FMRP, FXR1, and FXR2 crispants,
474 however, we found that FXR1 and FXR2 are dispensable but that FMRP is required for normal
475 startle sensitivity (Fig. 1F). This data is consistent with the distinct expression patterns of the
476 FMRP, FXR1 and FXR2 proteins, as well as the inability of FXR1/2 to functionally compensate

477 for the loss of FMRP [92–94]. Similarly, in *Drosophila*, which have only one Fragile X protein
478 family member (dFMR1), re-expressing human FMRP (hFMR1), but not human FXR1 or FXR2,
479 in dFMR1 mutants is sufficient to specifically rescue aberrant neuronal phenotypes [95]. As
480 discussed above, the fact that *fmr1* crispants but not *fmr1*^{hu2787} mutants show startle
481 hypersensitivity likely is due to genomic adaptation in the ENU-induced *fmr1*^{hu2787} line [50].
482 Furthermore, we observed that *fmr1* crispants show even further increased startle sensitivity in
483 the *cyfip2* mutant background compared to *cyfip2* mutants alone (Fig. 1F), strengthening our
484 conclusion that Cyfip2 and FMRP work cooperatively to regulate the startle threshold.
485
486 <u>Cyfip2-dependent branched actin dynamics are required for maintaining the acoustic startle</u>
487 <u>threshold.</u>
488 Our rescue experiments indicate that Cyfip2's actin regulatory function through its
489 binding with Rac1 is required during startle circuit development (Fig. 1E) and that this pathway
490 may also facilitate a more acute role for Cyfip2 in maintaining the startle threshold (Fig. 2A).
491 This conclusion is bolstered by our finding that inhibition of Arp2/3 with 20 μM CK-869 for 30
492 minutes prior to testing uncovers startle hypersensitivity in *cyfip2* heterozygotes but not
493 wildtypes (Fig. 2B). Thus in wildtypes, Cyfip2 must act acutely to facilitate actin polymerization
494 to maintain the startle threshold in the face of this challenge. Arp2/3-mediated F-actin nucleation
495 creates branched actin filaments, while formin-mediated nucleation produces unbranched
496 filaments [54–56,96]. Our data show that only branched actin nucleation is required for acute
497 maintenance of the startle threshold, while both formin activity and cofilin-mediated actin
498 filament severing play no acute role in regulating the startle threshold (Fig. 2C). Formin 2B has
499 been shown with morpholinos to be required developmentally for normal startle responsiveness,
500 however, and it appears to play a role in the growth of Spiral Fiber Neuron (SFN) axons [58].
501 SFNs are excitatory interneurons that receive input from the contralateral auditory nerve and
502 project their axons across the midline to the contralateral Mauthner cell, providing a key driving

503 force to initiate the startle response [97]. We previously found that SFNs, but not Mauthner cells,
504 have heightened excitability in *cyfip2* mutants [32], making them a likely place for Cyfip2 to
505 regulate the startle threshold. Functioning acutely, Cyfip2 may impact synaptic input onto SFNs,
506 and it is possible that inhibitory and/or excitatory synapses may be affected by Cyfip2 to
507 maintain the startle threshold. Cyfip1 and Cyfip2 are both enriched at excitatory synapses and
508 regulate dendritic complexity and spine maturation in mouse cortical neurons [82,83]. Both
509 Cyfip1 and Cyfip2 are also found at inhibitory postsynaptic sites in mouse hippocampal neurons,
510 and overexpression of either protein disrupts excitatory/inhibitory (E/I) synaptic balance [84]. It is
511 likely that Cyfip2 functions similarly in the zebrafish startle circuit to regulate neuronal
512 excitability, as our data implicate both excitatory (NMDA receptors; Fig. 2D) and inhibitory
513 (GABA receptors; Fig. 3B,E) pathways.
514
515 <u>Cyfip2 may control sensory processing and other disease-related functions by regulating</u>
516 <u>neurotransmitter receptors, mitochondrial function, and/or cytoskeletal remodeling.</u>
517 Our candidate drug screen to identify potential downstream effectors of Cyfip2 in
518 regulating the startle threshold builds on previous work showing that NMDA receptor function is
519 required for normal startle sensitivity (Fig 2D; Table 1) [59]. While our screen confirmed the
520 known roles of Cl^- and K^+ channels, gap junctions, calmodulin, and PDE4 in regulating startle
521 sensitivity, only the NMDA receptor blocker MK-801 produced a *cyfip2* genotype-specific
522 response, indicating that Cyfip2 may impact NMDA receptor expression and/or function in the
523 startle circuit. Our unbiased proteomic analysis of *cyfip2* heterozygotes and mutants did not
524 uncover dysregulation in excitatory synaptic function compared to wildtypes, although this may
525 be because we analyzed protein lysates from whole larvae and thus may have diluted out any
526 changes in NMDA receptor expression in specific neuronal subpopulations. It may also be the
527 case that Cyfip2 modulates the membrane localization of NMDA receptors through actin-
528 mediated trafficking rather than impacting total expression levels.

529 Ingenuity Pathway Analysis (IPA) of our proteomic data revealed that inhibitory GABA
530 receptor signaling is significantly disrupted in *cyfip2* heterozygotes and mutants (Fig. 3B). This
531 change most likely occurs through Cyfip2's translational regulation role via FMRP, although
532 further experiments are required to determine where and how Cyfip2 affects GABA receptor
533 expression. We did confirm that Cyfip2-mediated regulation of GABA receptor function plays a
534 key functional role in the startle threshold, showing that activation of $GABA_B$ but not $GABA_A$
535 receptors is sufficient to rescue the startle hypersensitivity phenotype in *cyfip2* mutants (Fig.
536 3D,E). Critically, the concentration of baclofen used did not affect wildtypes, and *cyfip2* mutant
537 startle sensitivity was reduced to the same level as in wildtypes, indicating that the rescue was
538 not due to a sedative effect. This result is consistent with recent findings using rats in which
539 baclofen-mediated activation of $GABA_B$ receptors restored normal auditory processing in
540 *Cntnap2* knockout animals [98]. $GABA_B$ receptors function both pre-synaptically to regulate
541 neurotransmitter release and post-synaptically to activate inward-rectifying K^+ channels that
542 cause hyperpolarization [99,100]. $GABA_B$ receptors are also expressed at high levels
543 throughout the auditory system [101], and baclofen treatment has been shown to improve social
544 avoidance in some individuals with autism [102–104]. It is currently unknown whether baclofen
545 affects sensory processing in clinical populations, however. Our data fit with a growing body of
546 evidence that $GABA_B$ receptors are critical modulators of auditory function with direct clinical
547 applications.
548 The most significantly disrupted pathways in our proteomic analysis of *cyfip2*
549 heterozygotes and mutants were oxidative phosphorylation and mitochondrial dysfunction (Fig.
550 3B). It is unclear if these metabolic functions influence the activity of the acoustic startle circuit,
551 although these pathways are essential within neurons for neuronal development and plasticity,
552 cell death, axon extension and branching, and synaptogenesis [105,106], and so they may also
553 contribute to the many disease associations for Cyfip2 listed above. Our data also show that in
554 the absence of Cyfip2, mitochondrial proteins (ACAD11, MT-ND4) increase in abundance, and

555 cytoskeletal (TMSB10/TMSB4X) and extracellular matrix (ECM) proteins (COL6A3, COL1A1)
556 decrease in abundance (Fig 3A; Table S8). TMSB4X and TMSB10 both suppress actin
557 polymerization [107,108], so their downregulation in *cyfip2* mutants may reflect an attempt to
558 compensate for the loss of Cyfip2- and WRC-mediated actin polymerization. ECM collagens like
559 COL6A3 and COL1A1 are important for multiple aspects of neural development including axon
560 guidance [109,110], and so this may reflect another potential mechanism for Cyfip2's
561 developmental role in regulating the startle circuit. Our analysis of diseases and functions
562 impacted by the loss of Cyfip2 include multiple neurological and neuromuscular conditions (Fig.
563 3C). These findings reinforce the known associations between *cyfip2* and diseases like ALS
564 [68,69] and Alzheimer's disease [70], further underscoring the central importance of Cyfip2 for
565 neural function beyond the startle circuit. Further work is needed to more clearly define the links
566 between Cyfip2, its molecular effectors, and the development, function, and maintenance of
567 neural circuits in order to improve our understanding of and ability to treat these varied
568 conditions.
569

570 **Materials & Methods**

571 Zebrafish Husbandry and Maintenance

572 All animal use and procedures were approved by the North Carolina State University
573 Institutional Animal Care and Use Committee (IACUC). Zebrafish embryos were obtained from
574 the Zebrafish International Resource Center (ZIRC), the University of Pennsylvania, or
575 generated at North Carolina State University and raised in a recirculating housing system.
576 Animals were fed and housed at a 5 zebrafish/L density under a 14h:10h light-dark cycle at
577 28°C.

578 Embryos were generated by a male and female pair placed in a mating box
579 (Aquaneering) containing system water and artificial grass. The following morning, 2-3 hours
580 into the light cycle, embryos were collected in petri dishes containing E3 embryo media (5 mM

581 NaCl, 0.17 mM KCl, 0.33 mM CaCl2·2H2O, 0.33 mM MgSO4 in water). Embryos were
582 examined under a brightfield compound microscope for fertilization and proper development and
583 were kept in groups ≤ 65. Embryos were placed in a 29˚C incubator on a 14h:10h light-dark
584 cycle. 50% of E3 media changed daily, and any embryos with gross morphological defects were
585 removed and euthanized.

586 DNA Extraction & Genotyping

587 Fin biopsies were obtained from adult fish anesthetized in 0.02% Tricaine (MS-222;
588 Fisher) in system water. Fin clips were taken using a razor blade to remove ~2-3 mm of tissue
589 from the tail fin and samples were immediately fixed in 100% MeOH. Larval samples were
590 individually fixed in 100% MeOH following behavioral testing. DNA was extracted using the
591 HotShot DNA lysis method which consisted of a tissue lysis with base solution (25mM NaOH,
592 0.2mM EDTA), sample incubation at 95°C for 30 minutes, and sample neutralization with
593 neutralizing solution (40mM Tris-HCl).*cyfip2*^{p400} fish were genotyped using rhAmp SNP
594 Genotyping System (IDT). rhAmp SNP genotyping was carried out using *cyfip2* locus and allele
595 specific primers (Table S3) targeting the wildtype and *cyfip2*^{p400} alleles. Genotyping for
596 *Tg(hsp70:cyfip2-GFP), Tg(hsp70:cyfip2-(C179R)-GFP)* and *Tg(hsp70:cyfip2-(K723E)-GFP)* was
597 accomplished by PCR amplification with primers specific to GFP (Table S4) followed by agarose
598 gel electrophoresis.

599 Molecular Cloning

600 Alternative *cyfip2* rescue constructs (Δ*Rac1*; Δ*FMRP*) were generated from a pENTR
601 *cyfip2*-EGFP plasmid [32] using custom primers and the Q5 Site Directed Mutagenesis Kit
602 (NEB) to induce the desired C179R (Δ*Rac1*) and K723E (Δ*FMRP*) mutations. Mutagenesis was
603 confirmed using restriction digest and Sanger sequencing (Table S3). LR Gateway Cloning
604 (ThermoFisher) was used to insert the altered *cyfip2*-EGFPs into the pDEST I-SceI hsp70
605 destination vector. Transgenic lines were created by microinjection into 1-cell stage embryos

606 with a transgenesis mix containing phenol red, I-SceI enzyme, and the pDEST I-SceI
607 hsp70:*cyfip2*-(C179R)-EGFP or pDEST I-SceI hsp70:*cyfip2*-(K723E)-EGFP plasmid.

608 Inducible Heatshock Rescue & Imaging

609 Inducible expression of *cyfip2-EGFP,* as well as C179R and K723E variants, was
610 initiated at 30 hpf by placing dechorionated larvae into 96-well plates and incubating at 38°C for
611 15 or 40 minutes [32]. Following heatshock, larvae were returned to Petri dishes, and given 4
612 days of recovery at 29°C. GFP fluorescence was confirmed between 4-6 hours post-heatshock
613 for startle experiments using a Nikon SMZ25 stereo microscope with a GFP bandpass filter and
614 Lumen 200 fluorescence illumination system. For day 5 heatshock rescue experiments, larvae
615 were given 4 hours of recovery at 29°C prior to startle sensitivity testing.

616 For imaging experiments, larvae were treated as above for transgene expression at 30
617 hpf and at 29°C for 1 hour recovered in petri dishes in groups ≤ 65. After 1 hour of recovery
618 fluorescence was verified, and larvae were visualized using the stereo microscope system
619 described above and larval images were captured at 1-, 3-, 6-, 18-, 24-, 30-, and 42-hours post-
620 heatshock using a Nikon DS-Qi2 monochrome microscope camera. Image analysis was
621 conducted using FIJI (ImageJ) analysis software to manually define ROIs encompassing the
622 entire larval body, excluding the eye and auto fluorescent yolk sac. Fluorescence intensity
623 values reflect the mean gray values recorded for respective ROIs.

624 Chemical Exposures

625 For all exposures, groups of 10-20 larvae (5 dpf) were incubated for specified periods of
626 between 30 minutes and 16 hours within 35 mm Petri dishes in 2 mL of each drug solution.
627 Drug solutions remained on larvae during startle testing for 30 minutes to 1-hour exposures. For
628 16-hour incubations larvae first received fresh E3 prior to testing. Following incubation, larvae
629 were placed on the 6x6 acrylic testing grid and run through the acoustic startle assay. CK-869,
630 CK-666, MK-801, *N*-phenylanthranilic acid (NPAA), meclofenamic acid (MA),
631 phenoxybenzamine (POBA), etazolate (ETAZ), BMS 204352, muscimol, and baclofen were

632 obtained from Sigma-Aldrich. SMIFH2, IPA-3, GSK429286 and NSC23766 were acquired from
633 Tocris through Fisher Scientific.

634 Behavioral Assays

635 All larvae were tested at 5 days post-fertilization (dpf) unless otherwise stated. On the
636 day of testing, embryos were thoroughly screened for developmental defects, and those with
637 gross morphological defects were removed prior to behavior testing. *cyfip2*^{p400} larvae without
638 inflated swim bladders were not discarded, as *cyfip2* mutant larvae fail to inflate their swim
639 bladders [32]. Larvae were adapted to the testing arena lighting and temperature conditions for
640 30 minutes prior to testing. As previously described, the behavioral testing system consists of a
641 36-well acrylic grid attached to an acoustic-vibrational shaker (Bruel-Kjaer), a photron mini UX-
642 50 camera, LED lighting, InfraRed illuminator, and an acrylic IR diffuser [5,32,59].

643 To test the acoustic startle response, 5 dpf larvae were presented with 60 total stimuli
644 with a 20 second interstimulus interval (ISI), with 10 pseudo randomized trials at each of the
645 following 6 stimulus intensities: 13.6, 25.7, 29.2, 35.5, 39.6 and 53.6 dB. All stimuli were
646 calibrated using a PCB Piezotronics accelerometer (#355B04) and signal conditioner
647 (#482A21), and voltage outputs were converted to dB using the formula dB = 20 log (V/0.775)
648 [32].

649 Behavioral Analysis

650 All responses in the acoustic startle assay were tracked using FLOTE analysis software
651 [5,32,59]. Short latency C-bends (SLCs) were identified by FLOTE using defined kinematic
652 parameters (latency, turn angle, duration, and maximum angular velocity). Startle sensitivity was
653 calculated by measuring the SLC frequency at each of the six stimulus intensities during the 60-
654 stimulus startle assay. Sensitivity indices were defined as the area under the startle frequency
655 vs. stimulus intensity curve calculated using Prism software (GraphPad).

656 Larval Sample Preparation for Proteomics.

657 Larvae from incrosses of *cyfip2*$^{+/p400}$ carriers were raised as described above. At 3 dpf, DNA was
658 extracted from larvae using the Zebrafish Embryonic Genotyping (ZEG) apparatus (DanioLab).
659 ZEG samples were used for PCR amplification and then submitted for Sanger sequencing to
660 determine the genotype at the *cyfip2*^{p400} locus. At 5 dpf larvae were sorted into pools of 30
661 larvae for each genotype: homozygous wild type, *cyfip2*^{p400} heterozygous, and homozygous
662 mutant. Samples were snap frozen in liquid nitrogen and stored at -80˚C. They were then
663 resuspended and lysed in 100 µL ammonium bicarbonate (ABC; pH 8) containing 1% sodium
664 deoxycholate (SDC) using a Branson SLPe Sonicator (40:0.15;4C) delivering two 20 second
665 pulses at 20% amplitude intensity separated by 10 seconds between pulses. Lysates were
666 centrifuged at 10,000 rpm for 5 minutes at 4˚C, and the supernatants were retained and
667 quantified using Pierce BCA protein quantification (ThermoFisher; Cat #: 23225) and an
668 IMPLEN NP80 nanophotometer. Lysates were submitted the same-day to the Molecular
669 Education, Technology and Research Innovation Center (METRIC) at NC State University for
670 protein digestion and LC-MS.
671 Protein Digestion and LC-MS
672 Each lysed sample was normalized to 200 µg of protein in 200 µL of ABC/SDC solution.
673 Disulfide reduction was conducted by adding 15 µL 50 mM DTT and incubating at 56˚C for 30
674 minutes. 200 µL of 8M urea in 0.1 M Tris buffer (pH 8) was added and samples were transferred
675 to Vivicon 30kD Molecular Weight Cut-off (MWCO) filters. Samples were centrifuged at 12,000 x
676 g for 10 minutes at 21˚C. 200 µL of 8 M urea in 0.1 M Tris buffer (pH 8) was added to the top of
677 each filter, as well as 64 µL 55 mM iodoacetamide (IAA) solution and samples were incubated
678 for 1 hour in the dark at room temperature. Samples were centrifuged at 12,000 x g for 20
679 minutes. 100 µL of 2 M urea, 10 mM $CaCl_2$ in 0.1 M Tris buffer (pH 8) was added and samples
680 were centrifuged at 12,000 x g for 20 minutes. The previous step was repeated twice. 100 µL of
681 0.1 M Tris buffer (pH 7.5) was added and samples were centrifuged at 12,000 x g for 20-45
682 minutes. This step was repeated twice, with a 1-hour centrifuge period on the final spin. 200 µL

683 of 0.02 µg/mL trypsin in 0.1 M Tris buffer (pH 7.5) was added, and samples incubated overnight
684 at 37˚C. Following protein digestion with trypsin, samples were placed into fresh microcentrifuge
685 reservoirs, and 50 µL of quench solution (0.001% zwittergent3-16 in water, 1% formic acid) was
686 added and samples centrifuged at 12,000 x g for 1 hour. 450 µL quench solution was applied to
687 each filter and samples were centrifuged at 14,000 x g for 1 hour. Solutions were dried using a
688 speedvac concentrator and samples were stored dry until LC-MS. Samples were reconstituted
689 in 100 µL of mobile phase A (98% water, 2% acetonitrile, 0.1% formic acid) and peptides were
690 quantified via Pierce BCA assay. Samples were normalized to the lowest peptide concentration
691 for every sample and nanoLC-MS was conducted using a Thermo Orbitrap Exploris 480. This
692 work was performed in part by METRIC at NC State University, which is supported by the State
693 of North Carolina.

694 Proteomics data analysis

695 Shotgun proteomics raw files were processed and quantified with MaxQuant (version 2.2.0.0).
696 Briefly, the built-in Andromeda search engine scored MS2 spectra against fragment masses of
697 tryptic peptides derived from a *Danio rerio* reference proteome containing 93,351 entries
698 including isoforms (UniProt, accessed March 22, 2019). Our database search required variable
699 modifications (methionine oxidation and N-terminal acetylation) and a fixed modification
700 (cysteine carbamido-methylation) along with a minimum peptide length of 7 amino acids and
701 limited the search space to a maximum peptide mass of 4600 Da and a maximum of two missed
702 cleavages. The false discovery rate was controlled with a target-decoy approach at less than
703 1% for peptide spectrum matches and protein group identifications.

704 Bioinformatics

705 Label-Free quantification (LFQ) intensities from MaxQuant were imported into Perseus software
706 (version 2.0.7.0) and transformed to logarithmic scale with base two. Missing values were

707 replaced with values from the normal distribution, reducing the distributions to a factor of “0.3″
708 (width) and down-shifting by “1.8″ standard deviations while simulating random values to
709 replace the missing values. This protein quantification was used to measure the fold-enrichment
710 between *cyfip2*^{p400} heterozygous/homozygous and *cyfip2* wildtype groups. Statistical
711 significance was calculated using a two-way Student t-test and FPR ($p<0.05$). Differentially
712 expressed proteins (DEPs) were submitted to ingenuity pathway analysis (IPA) to identify their
713 function, specific processes, and related enriched pathways/diseases.

714 Statistical Methods

715 All statistical analyses were performed using Prism (GraphPad). All data sets were tested for
716 normality in Prism. Subsequent parametric or non-parametric tests and post-hoc analyses were
717 performed using Prism, and significance values ($p < 0.05$) were reported.
718

719 **Acknowledgements**

720 We would like to thank Leonard Collins and Taufika Williams from METRIC at NC State
721 University for their assistance with proteomic analysis. A special thank you to Kimberly Scofield
722 and Kara Carlson for proofreading the manuscript.

723

724 **Funding Disclosure**

725 We are grateful for financial support from the National Institute for Neurological Disease and
726 Stroke (R01-NS116354 to K.C.M.) and for seed funds provided by North Carolina State
727 University’s Center for Human Health and the Environment (CHHE) through a National Institute
728 of Environmental Health Science center grant (P30 ES025128).

729

Competing Interests

The authors declare that no competing interests exist.

References

1. Burgess HA, Granato M. Modulation of locomotor activity in larval zebrafish during light adaptation. J Exp Biol. 2007;210: 2526–2539. doi:10.1242/jeb.003939

2. Vagnoni E, Lourenco SF, Longo MR. Threat modulates perception of looming visual stimuli. Curr Biol. 2012;22: R826-7. doi:10.1016/j.cub.2012.07.053

3. Randlett O, Haesemeyer M, Forkin G, Shoenhard H, Schier AF, Engert F, et al. Distributed Plasticity Drives Visual Habituation Learning in Larval Zebrafish. Curr Biol. 2019;29: 1337-1345.e4. doi:10.1016/j.cub.2019.02.039

4. Geyer MA, Swerdlow NR, Mansbach RS, Braff DL. Startle response models of sensorimotor gating and habituation deficits in schizophrenia. Brain Res Bull. 1990;25: 485–498. doi:10.1016/0361-9230(90)90241-q

5. Burgess HA, Granato M. Sensorimotor gating in larval zebrafish. J Neurosci. 2007;27: 4984–4994. doi:27/18/4984 [pii]

6. Weidenmüller A, Kleineidam C, Tautz J. Collective control of nest climate parameters in bumblebee colonies. Anim Behav. 2002;63: 1065–1071. doi:10.1006/anbe.2002.3020

7. Weidenmuller A. The control of nest climate in bumblebee (Bombus terrestris) colonies: interindividual variability and self reinforcement in fanning response. Behav Ecol. 2004;15: 120–128. doi:10.1093/beheco/arg101

8. Ward AJW, Sumpter DJT, Couzin ID, Hart PJB, Krause J. Quorum decision-making facilitates information transfer in fish shoals. Proc Natl Acad Sci U S A. 2008;105: 6948–6953. doi:10.1073/pnas.0710344105

9. Cresci A, De Rosa R, Agnisola C. Assessing the Influence of Personality on Sensitivity to Magnetic Fields in Zebrafish. J Vis Exp. 2019. doi:10.3791/59229

10. Michel WC, Sanderson MJ, Olson JK, Lipschitz DL. Evidence of a novel transduction pathway mediating detection of polyamines by the zebrafish olfactory system. J Exp Biol. 2003;206: 1697–1706. doi:10.1242/jeb.00339

11. Dudova I, Vodicka J, Havlovicova M, Sedlacek Z, Urbanek T, Hrdlicka M. Odor detection threshold, but not odor identification, is impaired in children with autism. Eur Child Adolesc Psychiatry. 2011;20: 333–340. doi:10.1007/s00787-011-0177-1

12. Tavassoli T, Baron-Cohen S. Olfactory detection thresholds and adaptation in adults with autism spectrum condition. J Autism Dev Disord. 2012;42: 905–909. doi:10.1007/s10803-011-1321-y

13. Takahashi H, Tsuboi A. Olfactory avoidance test (mouse). Bio Protoc. 2017;7: e2153. doi:10.21769/BioProtoc.2153

14. Blakemore S-J, Tavassoli T, Calò S, Thomas RM, Catmur C, Frith U, et al. Tactile sensitivity in Asperger syndrome. Brain Cogn. 2006;61: 5–13. doi:10.1016/j.bandc.2005.12.013

15. Kohashi T, Oda Y. Initiation of Mauthner- or non-Mauthner-mediated fast escape evoked by different modes of sensory input. J Neurosci. 2008;28: 10641–10653. doi:10.1523/JNEUROSCI.1435-08.2008

16. DeLorey TM, Sahbaie P, Hashemi E, Li W-W, Salehi A, Clark DJ. Somatosensory and sensorimotor consequences associated with the heterozygous disruption of the autism candidate gene, Gabrb3. Behav Brain Res. 2011;216: 36–45. doi:10.1016/j.bbr.2010.06.032

17. Puts NAJ, Wodka EL, Tommerdahl M, Mostofsky SH, Edden RAE. Impaired tactile processing in children with autism spectrum disorder. J Neurophysiol. 2014;111: 1803–1811. doi:10.1152/jn.00890.2013

18. Armington JC. The electroretinogram, the visual evoked potential, and the area-luminance relation. Vision Res. 1968;8: 263–276. doi:10.1016/0042-6989(68)90014-x

19. Campbell FW, Maffei L. The influence of spatial frequency and contrast on the perception of moving patterns. Vision Res. 1981;21: 713–721. doi:10.1016/0042-6989(81)90080-8

20. Yilmaz M, Meister M. Rapid innate defensive responses of mice to looming visual stimuli. Curr Biol. 2013;23: 2011–2015. doi:10.1016/j.cub.2013.08.015

21. Wang Y, Wu W, Zhang X, Hu X, Li Y, Lou S, et al. A Mouse Model of Visual Perceptual Learning Reveals Alterations in Neuronal Coding and Dendritic Spine Density in the Visual Cortex. Front Behav Neurosci. 2016;10: 42. doi:10.3389/fnbeh.2016.00042

22. Bakker MJ, Tijssen MA, van der Meer JN, Koelman JH, Boer F. Increased whole-body auditory startle reflex and autonomic reactivity in children with anxiety disorders. J Psychiatry Neurosci. 2009;34: 314–322. Available: https://www.ncbi.nlm.nih.gov/pubmed/19568483

23. Han K, Chen H, Gennarino VA, Richman R, Lu H-C, Zoghbi HY. Fragile X-like behaviors and abnormal cortical dendritic spines in cytoplasmic FMR1-interacting protein 2-mutant mice. Hum Mol Genet. 2015;24: 1813–1823. doi:10.1093/hmg/ddu595

24. Takahashi H, Nakahachi T, Stickley A, Ishitobi M, Kamio Y. Relationship between physiological and parent-observed auditory over-responsiveness in children with typical development and those with autism spectrum disorders. Autism. 2018;22: 291–298. doi:10.1177/1362361316680497 [doi]

25. Grillon C, Ameli R, Goddard A, Woods SW, Davis M. Baseline and fear-potentiated startle in panic disorder patients. Biol Psychiatry. 1994;35: 431–439. doi:10.1016/0006-3223(94)90040-x

803 26. Grillon C, Davis M. Acoustic startle and anticipatory anxiety in humans: effects of monaural
804 right and left ear stimulation. Psychophysiology. 1995;32: 155–161. doi:10.1111/j.1469-
805 8986.1995.tb03307.x [doi]

806 27. Chamberlain PD, Rodgers J, Crowley MJ, White SE, Freeston MH, South M. A potentiated
807 startle study of uncertainty and contextual anxiety in adolescents diagnosed with autism
808 spectrum disorder. Mol Autism. 2013;4: 31. doi:10.1186/2040-2392-4-31

809 28. Kohl S, Heekeren K, Klosterkötter J, Kuhn J. Prepulse inhibition in psychiatric disorders--
810 apart from schizophrenia. J Psychiatr Res. 2013;47: 445–452.
811 doi:10.1016/j.jpsychires.2012.11.018

812 29. Eaton RC, Bombardieri RA, Meyer DL. The Mauthner-initiated startle response in teleost
813 fish. J Exp Biol. 1977;66: 65–81. doi:10.1242/jeb.66.1.65

814 30. Kimmel CB, Patterson J, Kimmel RO. The development and behavioral characteristics of
815 the startle response in the zebra fish. Dev Psychobiol. 1974;7: 47–60.
816 doi:10.1002/dev.420070109

817 31. Davis M, Gendelman DS, Tischler MD, Gendelman PM. A primary acoustic startle circuit:
818 lesion and stimulation studies. J Neurosci. 1982;2: 791–805. doi:10.1523/JNEUROSCI.02-
819 06-00791.1982

820 32. Marsden KC, Jain RA, Wolman MA, Echeverry FA, Nelson JC, Hayer KE, et al. A Cyfip2-
821 Dependent Excitatory Interneuron Pathway Establishes the Innate Startle Threshold. Cell
822 Rep. 2018;23: 878–887. doi:S2211-1247(18)30471-6 [pii]

823 33. Schenck A, Bardoni B, Moro A, Bagni C, Mandel JL. A highly conserved protein family
824 interacting with the fragile X mental retardation protein (FMRP) and displaying selective
825 interactions with FMRP-related proteins FXR1P and FXR2P. Proc Natl Acad Sci U S A.
826 2001;98: 8844–8849. doi:10.1073/pnas.151231598 [doi]

827 34. Napoli I, Mercaldo V, Boyl PP, Eleuteri B, Zalfa F, Rubeis SD, et al. The fragile X syndrome
828 protein represses activity-dependent translation through CYFIP1, a new 4E-BP. Cell.
829 2008;134: 1042–1054. doi:10.1016/j.cell.2008.07.031 [doi]

830 35. Kobayashi K, Kuroda S, Fukata M, Nakamura T, Nagase T, Nomura N, et al. p140Sra-1
831 (specifically Rac1-associated protein) is a novel specific target for Rac1 small GTPase. J
832 Biol Chem. 1998;273: 291–295. doi:10.1074/jbc.273.1.291 [doi]

833 36. Eden S, Rohatgi R, Podtelejnikov AV, Mann M, Kirschner MW. Mechanism of regulation of
834 WAVE1-induced actin nucleation by Rac1 and Nck. Nature. 2002;418: 790–793.
835 doi:10.1038/nature00859

836 37. Schenck A, Bardoni B, Langmann C, Harden N, Mandel JL, Giangrande A. CYFIP/Sra-1
837 controls neuronal connectivity in Drosophila and links the Rac1 GTPase pathway to the
838 fragile X protein. Neuron. 2003;38: 887–898. doi:S0896627303003544 [pii]

839 38. Bogdan S, Grewe O, Strunk M, Mertens A, Klämbt C. Sra-1 interacts with Kette and Wasp
840 and is required for neuronal and bristle development in Drosophila. Development.
841 2004;131: 3981–3989. doi:10.1242/dev.01274

842 39. Chen Z, Borek D, Padrick SB, Gomez TS, Metlagel Z, Ismail AM, et al. Structure and
843 control of the actin regulatory WAVE complex. Nature. 2010;468: 533–538.
844 doi:10.1038/nature09623 [doi]

845 40. Chen B, Padrick SB, Henry L, Rosen MK. Biochemical reconstitution of the WAVE
846 regulatory complex. Methods Enzymol. 2014;540: 55–72. doi:10.1016/B978-0-12-397924-
847 7.00004-2

848 41. Chen B, Chou HT, Brautigam CA, Xing W, Yang S, Henry L, et al. Rac1 GTPase activates
849 the WAVE regulatory complex through two distinct binding sites. Elife. 2017;6:
850 10.7554/eLife.29795. doi:10.7554/eLife.29795 [doi]

851 42. Trowe T, Klostermann S, Baier H, Granato M, Crawford AD, Grunewald B, et al. Mutations
852 disrupting the ordering and topographic mapping of axons in the retinotectal projection of
853 the zebrafish, Danio rerio. Development. 1996;123: 439–450. doi:10.1242/dev.123.1.439

854 43. Schenck A, Qurashi A, Carrera P, Bardoni B, Diebold C, Schejter E, et al. WAVE/SCAR, a
855 multifunctional complex coordinating different aspects of neuronal connectivity. Dev Biol.
856 2004;274: 260–270. doi:10.1016/j.ydbio.2004.07.009

857 44. Pittman AJ, Gaynes JA, Chien CB. Nev (Cyfip2) is Required for Retinal Lamination and
858 Axon Guidance in the Zebrafish Retinotectal System. Dev Biol. 2010;344: 784–794.
859 doi:10.1016/j.ydbio.2010.05.512 [doi]

860 45. Cioni JM, Wong HH, Bressan D, Kodama L, Harris WA, Holt CE. Axon-Axon Interactions
861 Regulate Topographic Optic Tract Sorting via CYFIP2-Dependent WAVE Complex
862 Function. Neuron. 2018;97: 1078-1093.e6. doi:S0896-6273(18)30052-7 [pii]

863 46. Lee Y, Kim D, Ryu JR, Zhang Y, Kim S, Kim Y, et al. Phosphorylation of CYFIP2, a
864 component of the WAVE-regulatory complex, regulates dendritic spine density and neurite
865 outgrowth in cultured hippocampal neurons potentially by affecting the complex assembly.
866 Neuroreport. 2017;28: 749–754. doi:10.1097/WNR.0000000000000838

867 47. Zhang Y, Kang Hyae R, Lee S-H, Kim Y, Ma R, Jin C, et al. Enhanced Prefrontal Neuronal
868 Activity and Social Dominance Behavior in Postnatal Forebrain Excitatory Neuron-Specific
869 Cyfip2 Knock-Out Mice. Front Mol Neurosci. 2020;13: 574947.
870 doi:10.3389/fnmol.2020.574947

871 48. Kumar V, Kim K, Joseph C, Kourrich S, Yoo SH, Huang HC, et al. C57BL/6N mutation in
872 cytoplasmic FMRP interacting protein 2 regulates cocaine response. Science. 2013;342:
873 1508–1512. doi:10.1126/science.1245503 [doi]

874 49. Abekhoukh S, Bardoni B. CYFIP family proteins between autism and intellectual disability:
875 links with Fragile X syndrome. Front Cell Neurosci. 2014;8: 81.
876 doi:10.3389/fncel.2014.00081 [doi]

877 50. Barthelson K, Baer L, Dong Y, Hand M, Pujic Z, Newman M, et al. Zebrafish chromosome
878 14 gene differential expression in the fmr1 h u2787 model of Fragile X syndrome. Front
879 Genet. 2021;12: 625466. doi:10.3389/fgene.2021.625466

880 51. Hu J, Chen L, Yin J, Yin H, Huang Y, Tian J. Hyperactivity, memory defects, and
881 craniofacial abnormalities in zebrafish fmr1 mutant larvae. Behav Genet. 2020;50: 152–
882 160. doi:10.1007/s10519-020-09995-7

883 52. Spence EF, Soderling SH. Actin Out: Regulation of the Synaptic Cytoskeleton. J Biol
884 Chem. 2015;290: 28613–28622. doi:10.1074/jbc.R115.655118 [doi]

885 53. Chalkia D, Nikolaidis N, Makalowski W, Klein J, Nei M. Origins and evolution of the formin
886 multigene family that is involved in the formation of actin filaments. Mol Biol Evol. 2008;25:
887 2717–2733. doi:10.1093/molbev/msn215

888 54. Pellegrin S, Mellor H. The Rho family GTPase Rif induces filopodia through mDia2. Curr
889 Biol. 2005;15: 129–133. doi:10.1016/j.cub.2005.01.011

890 55. Schirenbeck A, Bretschneider T, Arasada R, Schleicher M, Faix J. The Diaphanous-related
891 formin dDia2 is required for the formation and maintenance of filopodia. Nat Cell Biol.
892 2005;7: 619–625. doi:10.1038/ncb1266

893 56. Peng J, Wallar BJ, Flanders A, Swiatek PJ, Alberts AS. Disruption of the Diaphanous-
894 related formin Drf1 gene encoding mDia1 reveals a role for Drf3 as an effector for Cdc42.
895 Curr Biol. 2003;13: 534–545. doi:10.1016/s0960-9822(03)00170-2

896 57. Maciver SK, Hussey PJ. The ADF/cofilin family: actin-remodeling proteins. Genome Biol.
897 2002;3: reviews3007. doi:10.1186/gb-2002-3-5-reviews3007

898 58. Nagar D, James TK, Mishra R, Guha S, Burgess SM, Ghose A. The Formin Fmn2b Is
899 Required for the Development of an Excitatory Interneuron Module in the Zebrafish
900 Acoustic Startle Circuit. eNeuro. 2021;8. doi:10.1523/ENEURO.0329-20.2021

901 59. Wolman MA, Jain RA, Liss L, Granato M. Chemical modulation of memory formation in
902 larval zebrafish. Proc Natl Acad Sci U S A. 2011;108: 15468–15473.
903 doi:10.1073/pnas.1107156108 [doi]

904 60. Focking M, Lopez LM, English JA, Dicker P, Wolff A, Brindley E, et al. Proteomic and
905 genomic evidence implicates the postsynaptic density in schizophrenia. Mol Psychiatry.
906 2015;20: 424–432. doi:10.1038/mp.2014.63 [doi]

907 61. Hoeffer CA, Sanchez E, Hagerman RJ, Mu Y, Nguyen DV, Wong H, et al. Altered mTOR
908 signaling and enhanced CYFIP2 expression levels in subjects with fragile X syndrome.
909 Genes Brain Behav. 2012;11: 332–341. doi:10.1111/j.1601-183X.2012.00768.x [doi]

910 62. Noroozi R, Omrani MD, Sayad A, Taheri M, Ghafouri-Fard S. Cytoplasmic FMRP
911 interacting protein 1/2 (CYFIP1/2) expression analysis in autism. Metab Brain Dis. 2018;33:
912 1353–1358. doi:10.1007/s11011-018-0249-8 [doi]

913 63. Zweier M, Begemann A, McWalter K, Cho MT, Abela L, Banka S, et al. Spatially clustering
914 de novo variants in CYFIP2, encoding the cytoplasmic FMRP interacting protein 2, cause
915 intellectual disability and seizures. Eur J Hum Genet. 2019;27: 747–759.
916 doi:10.1038/s41431-018-0331-z

917 64. Kirkpatrick SL, Goldberg LR, Yazdani N, Babbs RK, Wu J, Reed ER, et al. Cytoplasmic
918 FMR1-Interacting Protein 2 Is a Major Genetic Factor Underlying Binge Eating. Biol
919 Psychiatry. 2017;81: 757–769. doi:10.1016/j.biopsych.2016.10.021

920 65. Babbs RK, Beierle JA, Ruan QT, Kelliher JC, Chen MM, Feng AX, et al. Cyfip1
921 Haploinsufficiency Increases Compulsive-Like Behavior and Modulates Palatable Food
922 Intake in Mice: Dependence on Cyfip2 Genetic Background, Parent-of Origin, and Sex. G3
923 . 2019;9: 3009–3022. doi:10.1534/g3.119.400470

924 66. Babbs RK, Beierle JA, Yao EJ, Kelliher JC, Medeiros AR, Anandakumar J, et al. The effect
925 of the demyelinating agent cuprizone on binge-like eating of sweetened palatable food in
926 female and male C57BL/6 substrains. Appetite. 2020;150: 104678.
927 doi:10.1016/j.appet.2020.104678

928 67. Manigandan S, Yun JW. Loss of cytoplasmic FMR1-interacting protein 2 (CYFIP2) induces
929 browning in 3T3-L1 adipocytes via repression of GABA-BR and activation of mTORC1. J
930 Cell Biochem. 2022;123: 863–877. doi:10.1002/jcb.30231

931 68. Nachmany H, Wald S, Abekasis M, Bulvik S, Weil M. Two potential biomarkers identified in
932 mesenchymal stem cells and leukocytes of patients with sporadic amyotrophic lateral
933 sclerosis. Dis Markers. 2012;32: 211–220. doi:10.3233/DMA-2011-0885

934 69. Lilo E, Wald-Altman S, Solmesky LJ, Ben Yaakov K, Gershoni-Emek N, Bulvik S, et al.
935 Characterization of human sporadic ALS biomarkers in the familial ALS transgenic
936 mSOD1(G93A) mouse model. Hum Mol Genet. 2013;22: 4720–4725.
937 doi:10.1093/hmg/ddt325

938 70. Tiwari SS, Mizuno K, Ghosh A, Aziz W, Troakes C, Daoud J, et al. Alzheimer-related
939 decrease in CYFIP2 links amyloid production to tau hyperphosphorylation and memory
940 loss. Brain. 2016;139: 2751–2765. doi:10.1093/brain/aww205

941 71. Nakashima M, Kato M, Aoto K, Shiina M, Belal H, Mukaida S, et al. De novo hotspot
942 variants in CYFIP2 cause early-onset epileptic encephalopathy. Ann Neurol. 2018;83: 794–
943 806. doi:10.1002/ana.25208 [doi]

944 72. Begemann A, Sticht H, Begtrup A, Vitobello A, Faivre L, Banka S, et al. New insights into
945 the clinical and molecular spectrum of the novel CYFIP2-related neurodevelopmental
946 disorder and impairment of the WRC-mediated actin dynamics. Genet Med. 2021;23: 543–
947 554. doi:10.1038/s41436-020-01011-x

948 73. Biembengut ÍV, Silva ILZ, Souza T de ACB de, Shigunov P. Cytoplasmic FMR1 interacting
949 protein (CYFIP) family members and their function in neural development and disorders.
950 Mol Biol Rep. 2021;48: 6131–6143. doi:10.1007/s11033-021-06585-6

951 74. Biembengut ÍV, Shigunov P, Frota NF, Lourenzoni MR, de Souza TACB. Molecular
952 Dynamics of CYFIP2 Protein and Its R87C Variant Related to Early Infantile Epileptic
953 Encephalopathy. Int J Mol Sci. 2022;23. doi:10.3390/ijms23158708

954 75. Takahashi H, Nemoto T, Yoshida T, Honda H, Hasegawa T. Cancer diagnosis marker
955 extraction for soft tissue sarcomas based on gene expression profiling data by using

956 projective adaptive resonance theory (PART) filtering method. BMC Bioinformatics. 2006;7:
957 399. doi:10.1186/1471-2105-7-399

958 76. Mongroo PS, Noubissi FK, Cuatrecasas M, Kalabis J, King CE, Johnstone CN, et al. IMP-1
959 displays cross-talk with K-Ras and modulates colon cancer cell survival through the novel
960 proapoptotic protein CYFIP2. Cancer Res. 2011;71: 2172–2182. doi:10.1158/0008-
961 5472.CAN-10-3295

962 77. Jiao S, Li N, Cai S, Guo H, Wen Y. Inhibition of CYFIP2 promotes gastric cancer cell
963 proliferation and chemoresistance to 5-fluorouracil through activation of the Akt signaling
964 pathway. Oncol Lett. 2017;13: 2133–2140. doi:10.3892/ol.2017.5743

965 78. Vandamme T, Beyens M, Boons G, Schepers A, Kamp K, Biermann K, et al. Hotspot
966 DAXX, PTCH2 and CYFIP2 mutations in pancreatic neuroendocrine neoplasms. Endocr
967 Relat Cancer. 2019;26: 1–12. doi:10.1530/ERC-18-0120

968 79. Liu Y, Liu H, Bian Q. Identification of Potential Biomarkers Associated with Basal Cell
969 Carcinoma. Biomed Res Int. 2020;2020: 2073690. doi:10.1155/2020/2073690

970 80. Li Y, Song X, Liu L, Yue L. NUAK2 silencing inhibits the proliferation, migration and
971 epithelial-to-mesenchymal transition of cervical cancer cells via upregulating CYFIP2. Mol
972 Med Rep. 2021;24. doi:10.3892/mmr.2021.12457

973 81. Steffen A, Rottner K, Ehinger J, Innocenti M, Scita G, Wehland J, et al. Sra-1 and Nap1 link
974 Rac to actin assembly driving lamellipodia formation. EMBO J. 2004;23: 749–759.
975 doi:10.1038/sj.emboj.7600084

976 82. Rubeis SD, Pasciuto E, Li KW, Fernandez E, Marino DD, Buzzi A, et al. CYFIP1
977 coordinates mRNA translation and cytoskeleton remodeling to ensure proper dendritic
978 spine formation. Neuron. 2013;79: 1169–1182. doi:10.1016/j.neuron.2013.06.039 [doi]

979 83. Pathania M, Davenport EC, Muir J, Sheehan DF, Lopez-Domenech G, Kittler JT. The
980 autism and schizophrenia associated gene CYFIP1 is critical for the maintenance of
981 dendritic complexity and the stabilization of mature spines. Transl Psychiatry. 2014;4:
982 e374. doi:10.1038/tp.2014.16 [doi]

983 84. Davenport EC, Szulc BR, Drew J, Taylor J, Morgan T, Higgs NF, et al. Autism and
984 Schizophrenia-Associated CYFIP1 Regulates the Balance of Synaptic Excitation and
985 Inhibition. Cell Rep. 2019;26: 2037-2051.e6. doi:S2211-1247(19)30129-9 [pii]

986 85. Hanneman E, Trevarrow B, Metcalfe WK, Kimmel CB, Westerfield M. Segmental pattern of
987 development of the hindbrain and spinal cord of the zebrafish embryo. Development.
988 1988;103: 49–58. doi:10.1242/dev.103.1.49

989 86. Eaton RC, Farley RD. Development of the mauthner neurons in embryos and larvae of the
990 zebrafish, Brachydanio rerio. Copeia. 1973;1973: 673. doi:10.2307/1443067

991 87. Kimmel CB, Hatta K, Metcalfe WK. Early axonal contacts during development of an
992 identified dendrite in the brain of the zebrafish. Neuron. 1990;4: 535–545.
993 doi:10.1016/0896-6273(90)90111-r

994 88. Kimmel CB, Sessions SK, Kimmel RJ. Morphogenesis and synaptogenesis of the zebrafish
995 Mauthner neuron. J Comp Neurol. 1981;198: 101–120. doi:10.1002/cne.901980110

996 89. Tanimoto M, Ota Y, Horikawa K, Oda Y. Auditory input to CNS is acquired coincidentally
997 with development of inner ear after formation of functional afferent pathway in zebrafish. J
998 Neurosci. 2009;29: 2762–2767. doi:10.1523/JNEUROSCI.5530-08.2009

999 90. Siomi MC, Siomi H, Sauer WH, Srinivasan S, Nussbaum RL, Dreyfuss G. FXR1, an
1000 autosomal homolog of the fragile X mental retardation gene. EMBO J. 1995;14: 2401–
1001 2408. doi:10.1002/j.1460-2075.1995.tb07237.x

1002 91. Zhang Y, O'Connor JP, Siomi MC, Srinivasan S, Dutra A, Nussbaum RL, et al. The fragile
1003 X mental retardation syndrome protein interacts with novel homologs FXR1 and FXR2.
1004 EMBO J. 1995;14: 5358–5366. doi:10.1002/j.1460-2075.1995.tb00220.x

1005 92. Bakker CE, de Diego Otero Y, Bontekoe C, Raghoe P, Luteijn T, Hoogeveen AT, et al.
1006 Immunocytochemical and biochemical characterization of FMRP, FXR1P, and FXR2P in
1007 the mouse. Exp Cell Res. 2000;258: 162–170. doi:10.1006/excr.2000.4932

1008 93. Agulhon C, Blanchet P, Kobetz A, Marchant D, Faucon N, Sarda P, et al. Expression of
1009 FMR1, FXR1, and FXR2 genes in human prenatal tissues. J Neuropathol Exp Neurol.
1010 1999;58: 867–880. doi:10.1097/00005072-199908000-00009

1011 94. Tucker B, Richards R, Lardelli M. Expression of three zebrafish orthologs of human FMR1-
1012 related genes and their phylogenetic relationships. Dev Genes Evol. 2004;214: 567–574.
1013 doi:10.1007/s00427-004-0438-9

1014 95. Coffee RL Jr, Tessier CR, Woodruff EA 3rd, Broadie K. Fragile X mental retardation protein
1015 has a unique, evolutionarily conserved neuronal function not shared with FXR1P or
1016 FXR2P. Dis Model Mech. 2010;3: 471–485. doi:10.1242/dmm.004598

1017 96. Boczkowska M, Rebowski G, Kast DJ, Dominguez R. Structural analysis of the transitional
1018 state of Arp2/3 complex activation by two actin-bound WCAs. Nat Commun. 2014;5: 3308.
1019 doi:10.1038/ncomms4308

1020 97. Lacoste AM, Schoppik D, Robson DN, Haesemeyer M, Portugues R, Li JM, et al. A
1021 convergent and essential interneuron pathway for Mauthner-cell-mediated escapes. Curr
1022 Biol. 2015;25: 1526–1534. doi:10.1016/j.cub.2015.04.025 [doi]

1023 98. Möhrle D, Wang W, Whitehead SN, Schmid S. GABAB Receptor Agonist R-Baclofen
1024 Reverses Altered Auditory Reactivity and Filtering in the Cntnap2 Knock-Out Rat. Front
1025 Integr Neurosci. 2021;15. doi:10.3389/fnint.2021.710593

1026 99. Waldmeier PC, Kaupmann K, Urwyler S. Roles of GABAB receptor subtypes in presynaptic
1027 auto- and heteroreceptor function regulating GABA and glutamate release. J Neural
1028 Transm. 2008;115: 1401–1411. doi:10.1007/s00702-008-0095-7

1029 100. Wu C, Sun D. GABA receptors in brain development, function, and injury. Metab Brain
1030 Dis. 2015;30: 367–379. doi:10.1007/s11011-014-9560-1

1031 101. Tureček R, Melichar A, Králíková M, Hrušková B. The role of GABAB receptors in the
1032 subcortical pathways of the mammalian auditory system. Front Endocrinol . 2023;14:
1033 1195038. doi:10.3389/fendo.2023.1195038

1034 102. Berry-Kravis E, Hagerman R, Visootsak J, Budimirovic D, Kaufmann WE, Cherubini M,
1035 et al. Arbaclofen in fragile X syndrome: results of phase 3 trials. J Neurodev Disord.
1036 2017;9: 3. doi:10.1186/s11689-016-9181-6

1037 103. Veenstra-VanderWeele J, Cook EH, King BH, Zarevics P, Cherubini M, Walton-Bowen
1038 K, et al. Arbaclofen in Children and Adolescents with Autism Spectrum Disorder: A
1039 Randomized, Controlled, Phase 2 Trial. Neuropsychopharmacology. 2017;42: 1390–1398.
1040 doi:10.1038/npp.2016.237

1041 104. Erickson CA, Veenstra-Vanderweele JM, Melmed RD, McCracken JT, Ginsberg LD,
1042 Sikich L, et al. STX209 (arbaclofen) for autism spectrum disorders: an 8-week open-label
1043 study. J Autism Dev Disord. 2014;44: 958–964. doi:10.1007/s10803-013-1963-z

1044 105. Mattson MP, Gleichmann M, Cheng A. Mitochondria in neuroplasticity and neurological
1045 disorders. Neuron. 2008;60: 748–766. doi:10.1016/j.neuron.2008.10.010

1046 106. Smith GM, Gallo G. The role of mitochondria in axon development and regeneration.
1047 Dev Neurobiol. 2018;78: 221–237. doi:10.1002/dneu.22546

1048 107. Safer D, Elzinga M, Nachmias VT. Thymosin beta 4 and Fx, an actin-sequestering
1049 peptide, are indistinguishable. J Biol Chem. 1991;266: 4029–4032. Available:
1050 https://www.ncbi.nlm.nih.gov/pubmed/1999398

1051 108. Yu FX, Lin SC, Morrison-Bogorad M, Atkinson MA, Yin HL. Thymosin beta 10 and
1052 thymosin beta 4 are both actin monomer sequestering proteins. J Biol Chem. 1993;268:
1053 502–509. doi:10.1016/s0021-9258(18)54179-x

1054 109. Cheng IH, Lin Y-C, Hwang E, Huang H-T, Chang W-H, Liu Y-L, et al. Collagen VI
1055 protects against neuronal apoptosis elicited by ultraviolet irradiation via an
1056 Akt/phosphatidylinositol 3-kinase signaling pathway. Neuroscience. 2011;183: 178–188.
1057 doi:10.1016/j.neuroscience.2011.03.057

1058 110. Fox MA. Novel roles for collagens in wiring the vertebrate nervous system. Curr Opin
1059 Cell Biol. 2008;20: 508–513. doi:10.1016/j.ceb.2008.05.003

1060

1061

1062 **Figure Legends**

1063 **Figure 1. Cyfip2 establishes the acoustic startle threshold through Rac1 and FMRP.**

1064 (A) Cyfip2 protein interacting domain diagram of wildtype (top) and mutant (bottom) Cyfip2
1065 proteins. Black arrowheads indicate the positions of induced mutations in Cyfip2, eliminating the
1066 Rac1- (C179R) or FMRP/eIF4E (K723E)-binding capacity of Cyfip2. (B) Cyfip2 actin regulatory
1067 pathway wherein Cyfip2 (orange) upon stimulation by Rac1-GTP triggers WAVE1 activation,
1068 Arp2/3-complex initiation and branched actin nucleation. (C) Cyfip2 translational repression
1069 pathway in which Cyfip2, eIF4E (teal), and FMRP (pink) along with the poly-A binding protein
1070 (PABP; gray), sequester neurodevelopmentally important mRNAs from being translated. (D)
1071 Average startle frequency (%) after 10 trials at 13.6, 25.7, 29.2, 35.5, 39.6 and 53.6 dB for 5 dpf
1072 *cyfip2* siblings (+/) and mutant (-/-) larvae heatshocked at 30 hpf for 40 minutes at 38˚C. The
1073 average startle frequency curve for cyfip2 siblings (+/; open circles, dashed line), cyfip2 mutants
1074 (-/-; closed circles, solid line) and cyfip2 mutants harboring the *Tg(hsp70:cyfip2-EGFP)+*
1075 transgene (-/-; Tg+; closed circles, solid green line). (E) Sensitivity indices, calculated as the
1076 area under the startle frequency curves, for 5 dpf cyfip2 siblings and mutants, following a 40-
1077 minute heatshock at 30 hpf to express either wildtype (Tg+; green), Rac1- (ΔRac1+; blue) or
1078 FMRP/eIF4E- (ΔFMRP+; pink) binding deficient versions of Cyfip2-EGFP. Comparisons were
1079 made to both non-transgenic (Tg-) and non-heatshocked controls. All indices (mean ± SD)
1080 compared using a Kruskal-Wallis test with Dunn's multiple comparisons correction; p**** <
1081 0.0001. (F) Sensitivity indices for 5 dpf *cyfip2* sibling (+/) and mutant (-/-) larvae following 1-cell
1082 stage injection with CRISPR-Cas9 and a single, scrambled guide RNA (gRNA) or dual gRNA
1083 cocktails targeting *fmr1*, *fxr1*, or *fxr2*. scrambled gRNA injected (white bar, closed circles); fmr1
1084 gRNA injected (dark gray bar closed circles); *fxr1* gRNA injected (medium gray bar; closed
1085 circles); *fxr2* gRNA injected (light gray bar, closed circles). Comparisons were made both within
1086 genotype and between genotypes by condition. All indices (mean ± SD) compared using an
1087 Ordinary one-way ANOVA with Sidak's multiple comparisons correction; p* < 0.05; p** < 0.01;
1088 p**** < 0.0001.

1089

1090 **Figure 2. Cyfip2 acutely regulates branched actin polymerization and NMDARs to**

1091 **establish the acoustic startle threshold.**

1092 (A) Sensitivity indices for 5 dpf *cyfip2* sibling (+/) and mutant (-/-) larvae, following a 40-minute
1093 heatshock at 120 hpf (5 dpf) to express either wildtype (Tg+; green), Rac1- (ΔRac1+; blue) or
1094 FMRP/eIF4E- (ΔFMRP+; pink) binding deficient versions of Cyfip2-EGFP. Comparisons were
1095 made to non-transgenic (Tg-), heatshocked sibling (+/) and mutant (-/-) controls. All indices
1096 (mean ± SD) compared using a Kruskal-Wallis test with Dunn's multiple comparisons correction;
1097 p-values listed; p** < 0.01, p**** < 0.0001. (B) Sensitivity indices for 5 dpf *cyfip2* wildtype (+/+;
1098 white bar) and heterozygous (+/-; gray bar) larvae, treated for 30 minutes on d5 with 5, 20 or 50
1099 μM CK-869. Comparisons were made both within genotype and within condition. All indices
1100 (mean ± SD) compared using a Kruskal-Wallis test with Dunn's multiple comparisons correction;
1101 p* < 0.05; p**** < 0.0001. (C) Sensitivity indices for 5 dpf Tüpfel longfin (TL) larvae treated for
1102 30 minutes on d5 with the highest, non-lethal doses the formin antagonist (SMIFH2; 5 μM),
1103 PAK3 antagonist (IPA-3; 50 μM) and ROCK antagonist (GSK429286; 100 μM). Comparisons
1104 were made between respective treatments and the DMSO controls. All indices (mean ± SD)
1105 were compared using a Kruskal-Wallis test with Dunn's multiple comparisons correction; All
1106 comparisons made were non-significant (n.s.). (D) Sensitivity indices for 5 dpf *cyfip2* sibling (+/)
1107 and mutant (-/-) larvae, treated for 30 minutes on d5 with 100 or 500 μM MK-801. Comparisons
1108 were made both between genotypes within condition and between conditions by genotype. All
1109 indices (mean ± SD) were compared using an Ordinary one-way ANOVA with Tukey's multiple
1110 comparisons correction. p** < 0.01; p*** < 0.001; p**** < 0.0001.

1111

1112 **Figure 3. Loss of Cyfip2 causes widespread proteomic changes and GABAB receptor**

1113 **signaling is critical for startle sensitivity.**

1114 (A) Bubble plots reporting the level of significance of the top 10 dysregulated proteins for both

1115 *cyfip2* heterozygous (top) and mutant (bottom) groups compared to wildtype controls. The size

1116 of the dot is proportional to the significance of the results while the color code represents the

1117 log2 fold change; top five upregulated (green), and top five downregulated (red) proteins are

1118 shown. (B-C) Heat maps displaying the impacted canonical pathways (B) and diseases and

1119 biological functions (C) from IPA functional analysis. The blue-colored gradient indicates the

1120 degree of enrichment for the listed pathways or diseases/functions, as represented by the – log

1121 of the P value for each pathway, disease and/or function. (D-E) Sensitivity indices for 5 dpf

1122 *cyfip2* sibling (+/) and mutant (-/-) larvae, treated for 60 minutes prior to testing with muscimol

1123 (D) or (E) baclofen. All indices (mean ± SD) were compared using a one-way ANOVA with

1124 Sidak's multiple comparisons correction. p* < 0.05, p** < 0.01; p*** < 0.001; p**** < 0.0001.

1125

1126 **Tables**

Compound	Concentration (μM)	Effect By Genotype		
		cyfip2(+/+)	***cyfip2(+/-)***	***cyfip2(-/-)***
NPAA (Cl- channel antagonist)	1	93.21% of Control, p > 0.99	110.21% of Control, p < 0.99	113.57% of Control, p > 0.99
	5	140.11% of Control, p = 0.9785	137.32% of Control, p = 0.1385	140.29% of Control, p > 0.2787
	10	**234.14% of Control, p** = 0.0038**	**201.29% of Control, p**** < 0.0001**	**155.06% of Control, p* = 0.0189**
MA (K+ channel/gap jxn. antagonist)	1	131.6% of Control, p > 0.99	11.87% of Control, p > 0.99	132.29% of Control, p = 0.5732
	5	137.24% of Control, p > 0.99	138.46% of Control, p = 0.0622	112.29% of Control, p > 0.99
	10	214.13% of Control, p = 0.0833	**169.81% of Control, p* = 0.0188**	**155.76% of Control, p* = 0.0288**
POBA (AAR/calmodulin antagonist)	1	102.9% of Control, p > 0.99	107.08% of Control, p > 0.99	101.04% of Control, p > 0.99
	10	136.17% of Control, p > 0.99	106.58% of Control, p > 0.99	99.01% of Control, p > 0.99

	50	**175.8% of Control, p* = 0.0123**		99.76% of Control, p > 0.99
ETAZ (PDE4 inhibitor)	1	141.79% of Control, p > 0.99	126.36% of Control, p > 0.99	121.74% of Control, p > 0.99
	10	168.6% of Control, p = 0.5472	**172.26% of Control, p* = 0.0137**	152.73% of Control, p = 0.3977
	50	**236.64% of Control, p** = 0.0029**	**179.99% of Control, p** = 0.0015**	**149.75% of Control, p* = 0.0105**
MK-801 (NMDAR antagonist)	100	120.19% of Control, p > 0.99		**145.93% of Control, p** = 0.0024**
	500	**212.69% of Control, p**** < 0.0001**		**163.26% of Control, p*** = 0.0002**
BMS-204352 (K+ channel antagonist)	10	79.48% of Control, p = 0.4269		89.55% of Control, p > 0.99
	50	76.08% of Control, p = 0.6759		108.74% of Control, p > 0.99
NSC-23766 (Rac1 antagonist)	100	**49.14% of Control, p*** = 0.0002**		81.60% of Control, p > 0.99
	200	86.26% of Control, p > 0.99		105.28% of Control, p > 0.99

Table 1. Cyfip2 may regulate NMDARs to control acoustic startle sensitivity. Mean startle index comparisons, listed as percentage (%) of the mean startle index of vehicle-treated controls by *cyfip2* genotype and drug concentration, for larvae treated with compounds targeting the indicated pathways [59] to increase acoustic startle sensitivity. All significant differences ($p < 0.05$) are listed (**bold**) for comparisons using a Kruskal-Wallis test and Dunn's multiple comparisons correction. NPAA (*N*-phenylanthranilic acid); MA (meclofenamic acid); POBA (phenoxybenzamine); ETAZ (etazolate).

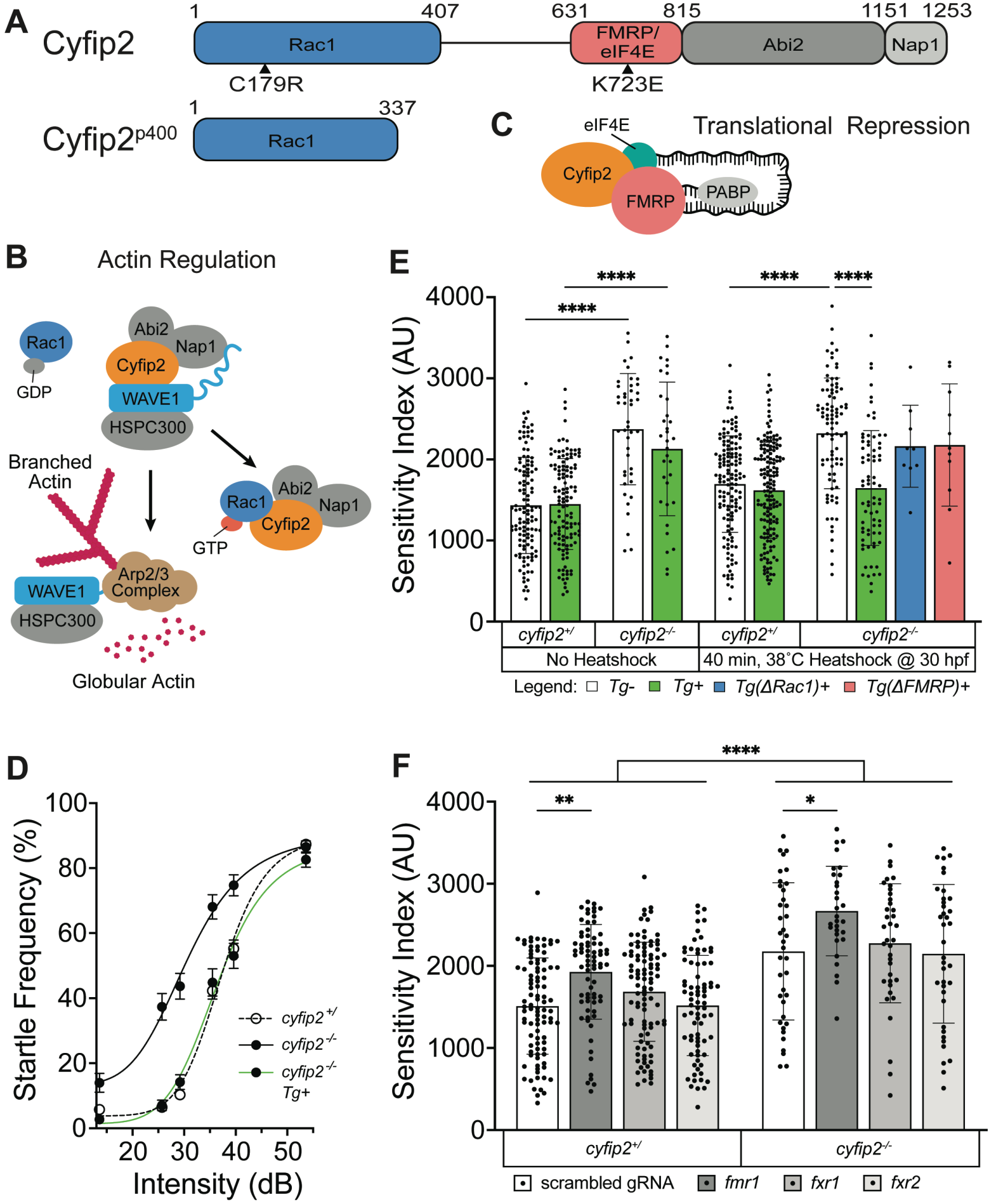

Figure 1 Deslauriers et al. 2023

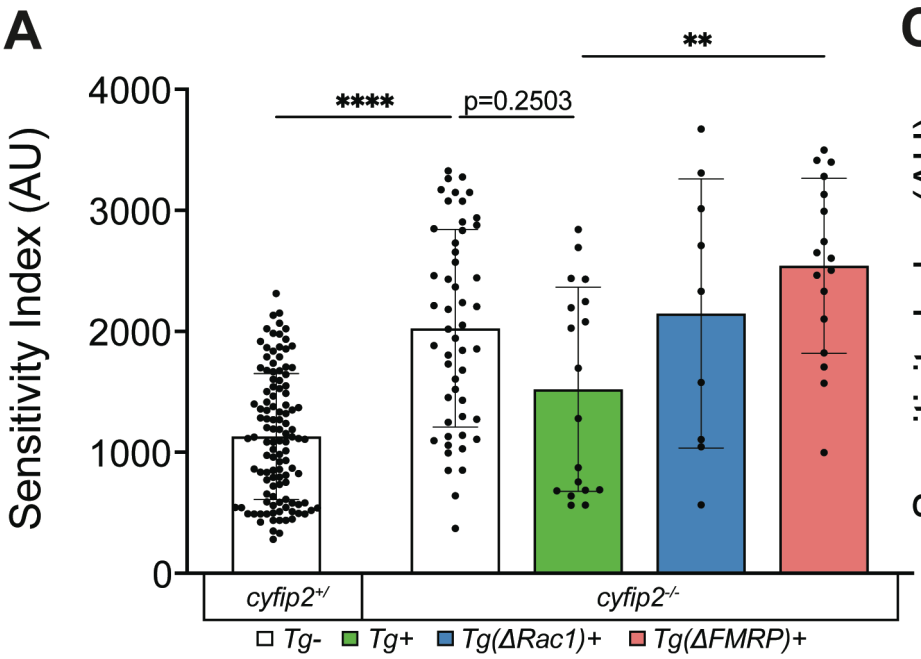

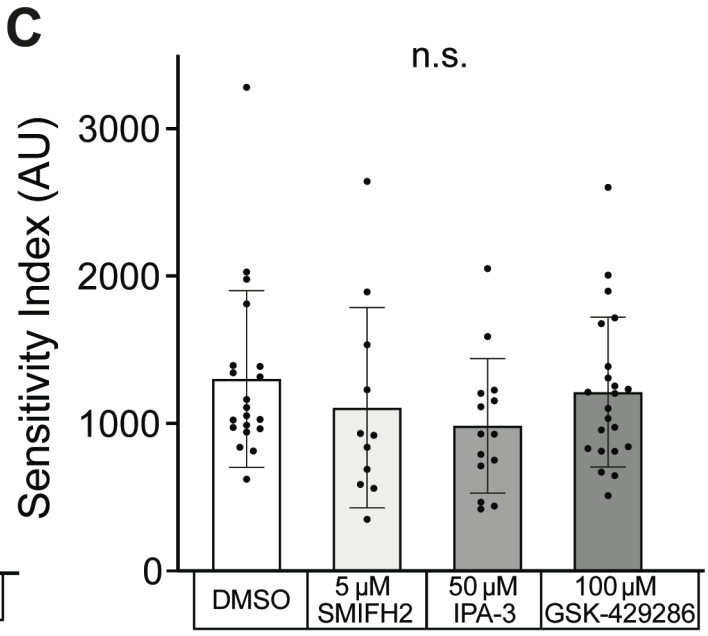

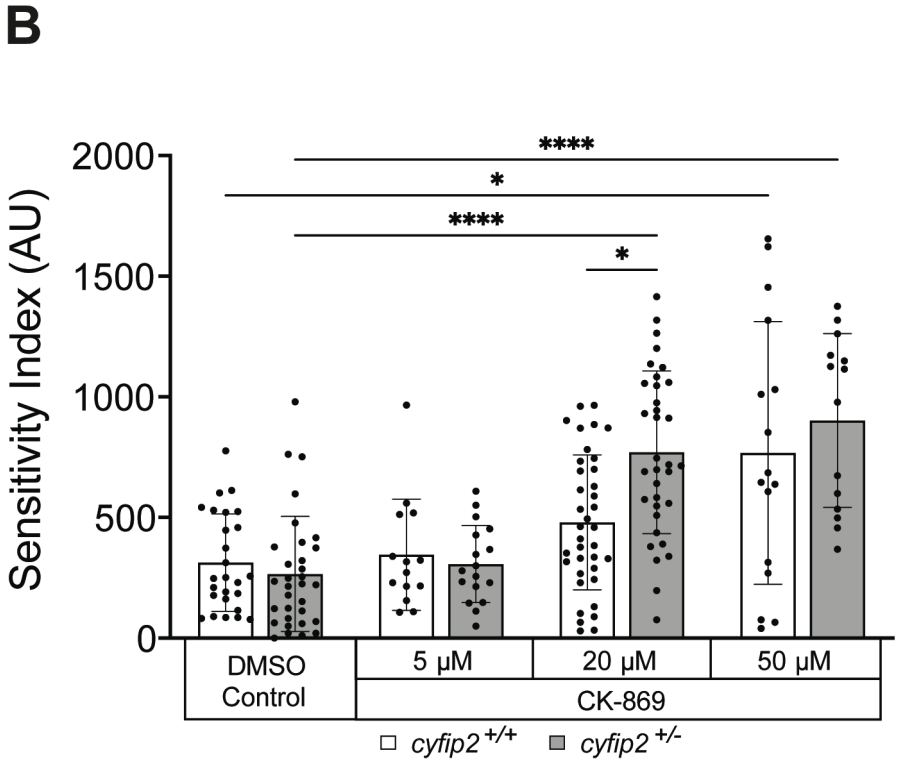

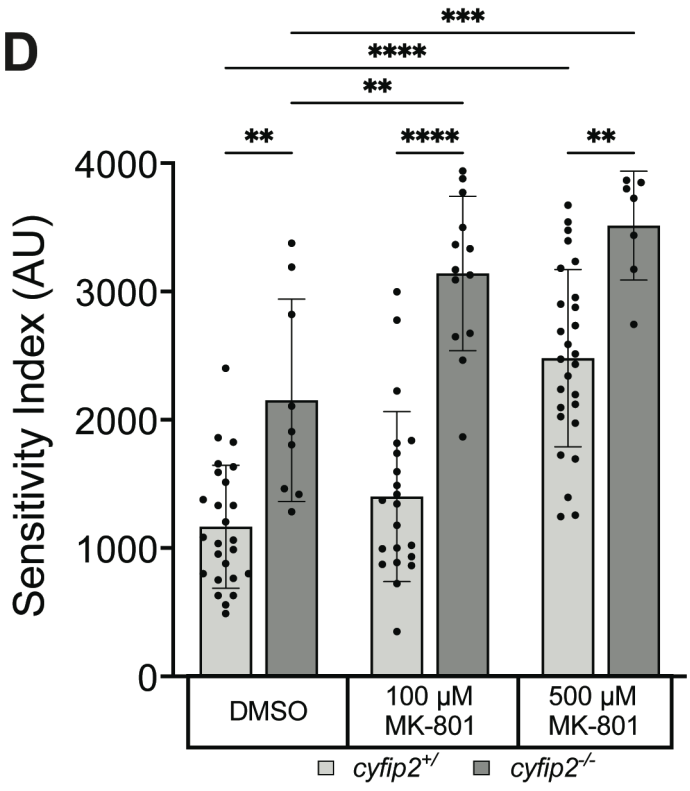

Figure 2 Deslauriers et al. 2023

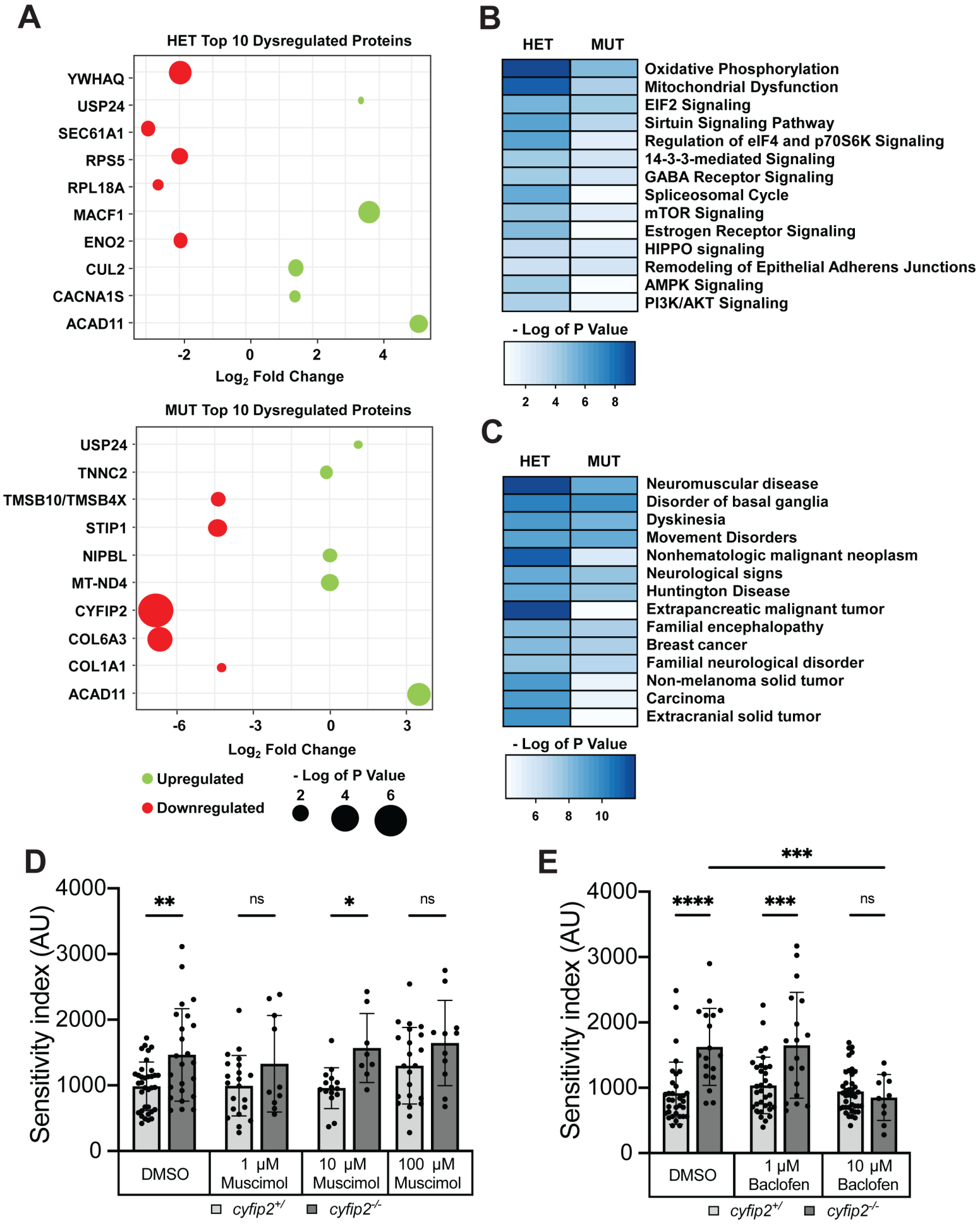

Figure 3 Deslauriers et al. 2023